Chemical characteristics of submicron particles at the central Tibet Plateau: ~~influence of long-range transport~~insights from aerosol mass spectrometry

Jianzhong Xu[1], Qi Zhang[2], Jinsen Shi[3], Xinlei Ge[4], Conghui Xie[1], Junfeng Wang[4], Shichang Kang[1], Ruxiong Zhang[5], Yuhang Wang[5]

[1]State Key Laboratory of Cryospheric Sciences, Northwest Institute of Eco-Environment and Resources, CAS, Lanzhou 730000, China

[2]Department of Environmental Toxicology, University of California, Davis, CA 95616, USA

[3]Key Laboratory for Semi-Arid Climate Change of the Ministry of Education, College of Atmospheric Sciences, Lanzhou University, Lanzhou 730000, China

[4]Jiangsu Key Laboratory of Atmospheric Environment Monitoring and Pollution Control (AEMPC), School of Environmental Science and Engineering, Nanjing University of Information Science & Technology, Nanjing 210044, China

[5]School of Earth and Atmospheric Sciences, Georgia Institute of Technology, Atlanta, GA, USA

Abstract

Recent studies have revealed a significant influx of air pollution from south Asia to Himalayas and Tibet Plateau (TP) during pre-monsoon period. In order to characterize the chemical composition, sources, and transport ~~mechanism~~processes of polluted air mass in this ~~pristine~~ area, we ~~performed~~carried out a field study during June 2015 by deploying a suite of online instruments including an Aerodyne high-resolution time-of-flight aerosol mass spectrometer (HR-AMS) and a multi-angle absorption photometer (MAAP) at Nam Co Station (90°57′E, 30°46′N, 4730m a.s.l) at the central of the TP. The measurements were made at a ~~time~~period when the transition from pre-monsoon to monsoon occurred. The average ambient mass concentration of submicron particulate matter (PM$_1$) over the whole campaign ~~period~~ was ~2.0 μg m^{-3}, with organics accounting for ~~64~~68%, followed by sulfate (~~16~~15%), black carbon (~~9~~8%), ammonium (~~8~~7%), and nitrate (~~3%). This mass loading and composition were comparable with most of AMS results in remote sites worldwide.~~2%). Air pollution episodes were observed during the pre-monsoon period, ~~while consistently~~whereas persistently low aerosol concentrations were observed during the monsoon period. However, the chemical composition of aerosol during the air pollution episodes in the pre-monsoon season was on a case-by-case basis, depending on the prevailing meteorological conditions and air mass transport routes. Most of the chemical species exhibited significant diurnal variations with higher values occurring during afternoon and lower values during early morning~~ time~~, whereas nitrate peaked during early morning in association with higher relative humidity and lower air temperature. Organic aerosol (OA) was more

oxidized with an oxygen-to-carbon ratio (O/C) of 0.94 during the pre-monsoon period than during monsoon (average O/C of 0.~~48~~72). The average O/C of OA was 0.88 over the entire campaign period. Positive matrix factorization of the high resolution mass spectra of OA identified two oxygenated organic aerosol (OOA) factors: a less oxidized OOA (LO-OOA) and a more oxidized OOA (MO-OOA). The MO-OOA dominated during the pre-monsoon period, ~~while~~whereas LO-OOA dominated during ~~the~~ monsoon. The sensitivity of air pollution transport with synoptic process was also evaluated with a 3-D chemical transport model.

1. Introduction

The Tibet Plateau (TP) and Himalayas is a vast and elevated highland in Central Asia that extends over the area of 27–45°N, 70–105°E with a mean elevation of more than 4000 m above sea level (a.s.l.). It is a sparsely populated area with minimal local pollution. The TP is an ideal area for observations of free tropospheric air masses and pollutants transported from polluted areas surrounding the TP after long-~~range transport.~~ distances. Determination of the chemical characteristics of aerosol particles in TP is important for ~~assessment on~~assessments of their ~~influence~~influences on atmospheric chemistry and climate (Li et al., 2016), which are so far poorly understood due to harsh conditions and logistic ~~limitation~~limitations.

Over recent decades, an increasing number of field studies have been conducted in these regions to characterize aerosol physical and chemical features from mountain observatories, e.g., the Nepal Climate Observatory-Pyramid (5079 m), which ~~are~~is set up for long-term monitoring and synchronous observation (Bonasoni et al., 2010; Liu et al., 2017). There are significant seasonal variations in aerosol mass loading in the southern TP and Himalayas. Higher aerosol concentration was often found during pre-monsoon due to less precipitation and favorable atmospheric circulation (Bonasoni et al., 2010; Marinoni et al., 2010; Marinoni et al., 2013; Zhao et al., 2013). For example, the concentration of carbonaceous species at the Qomolangma (Mt. Everest) Station (4276 m a.s.l.), northern Himalayas during pre-monsoon was found to be 3 – 5 times higher than that during the monsoon periods (Cong et al., 2015). ~~Since this seasonal variation of aerosol loading is consistent at both the southern and northern Himalayas (Xu et al., 2014), polluted air mass was thought to be able to across the Himalayas, a condition~~Since this seasonal variation of aerosol loading is consistent at both the southern and northern Himalayas (Xu et al., 2014a), polluted air mass was thought to be able to across the Himalayas, a finding which is also supported by model results (Lu et al., 2012; Lüthi et al., 2015; Zhang et al., 2015). During monsoon period, ambient aerosol ~~at~~ from the upwind sources is significantly scavenged ~~before~~during long-range transport and air mass ~~are~~is mainly originated from marine area, which ~~had~~can lead to aerosol chemical ~~difference~~differences between pre-monsoon and monsoon. The distinct seasonal variation of aerosol loading is mainly attributed to the change of the dominated climatic systems and then weather conditions. During pre-monsoon, the cold and dry southern Westliers dominated the southern TP and Himalayas, while the South Asia Monsoon covers most of South Asia, Himalayas, and the southern TP during summer period.

73

74 Most of the studies conducted in these regions focused on some specific species, such as black carbon,

75 which has ~~strongly~~strong light absorption. Burning of biomass fuels and wildfires in the south Himalaya

76 and South Asia are thought to be important sources for the black carbon (Stone et al., 2010; Engling et al.,

77 2011; Kumar et al., 2011). However, a recent study shows that sources of black carbon in the region of

78 South Asia are highly complex, including emissions from low efficient transport tools and cooking using

79 cow dung and biogas as well (Stockwell et al., 2016). These burning activities also emit other species such

80 as organic and inorganic particulate species and volatile organic compounds, which generate a well-mixed

81 aerosol plume eventually via processes such as coagulation, evaporation, oxidation, and condensation. Fang

82 et al. (2015) recently suspected that biogenic aerosol could also be an important contribution for aerosol in

83 the TP during summer. However, these mixed plumes have been rarely, if ever, characterized by

84 comprehensive field measurements.

85

86 Filter-based sampling method with a low time resolution (days) were widely adopt in these remote regions

87 due to logistical difficulties with deployment of real-time instruments. The low time resolution made the

88 understanding of chemical processes of aerosol during transport challenging. Secondary species such as

89 sulfate and water soluble organic carbon (WSOC) are normally the dominated species in aerosol. For

90 example, WSOC accounted for about 60% of OC and the ratio between OC and EC could be up to 10

91 (Zhao et al., 2013; Cong et al., 2015), suggesting a dominant contribution of secondary organic aerosol

92 (SOA) to carbonaceous aerosol loading in the TP. The ambient conditions at high elevation regions are

93 characterized by higher solar radiation and concentrations of oxidants such as OH radicals and O_3, which

94 ~~make~~makes photochemical processing in this high elevation remote region intense and likely ~~dynamic.~~

95 ~~Therefore high~~dominant. High-time resolution measurement is thus necessary in ~~these regions~~this region

96 for detecting short-term events and the evolution of ~~pollution events.~~pollutants. In addition, the high time

97 resolution data are useful for constraining atmospheric chemical transport models.

98

99 The aerodyne aerosol mass spectrometer (AMS) has been widely used to study the chemical composition of

100 non-refractory submicron particle~~.~~ (e.g., Xu et al., 2014b; Xu et al., 2016). There are two merits of the

101 AMS including its high time resolution and bulk measurement. The high time resolution is usually

102 ~~minute~~in minutes which has advanced our understanding of fundamental chemical ~~composition~~processes of

103 fine aerosols at different regions of the world (Canagaratna et al., 2007). The bulk measurements

104 ~~make~~enable the observation to obtain ~~more~~rich information of various aerosol ~~in one time.~~chemical species

105 simutaneously. The organic aerosol, which is often the most important component of aerosol, can be further

106 analyzed ~~for their mass spectra~~ to determine the average elemental ratios and by positive matrix

107 factorization (PMF) analysis to determine the sources and atmospheric processes ~~of aerosol~~ (Ulbrich et al.,

108 2009; Zhang et al., 2011). The atomic elemental ratios of oxygen and hydrogen ~~with~~to carbon (O~~:~~/C and

109 H~~:~~/C) calculated from the OA mass spectra can provide information about the sources and evolution

110 processes of OA in the atmosphere (Aiken et al., 2008; Heald et al., 2010; Kroll et al., 2011; Ng et al.,

111 2011). They also often closely correlate with key OA properties such as hygroscopicity, ~~material~~ density,

112 and phase separation (Jimenez et al., 2009; Bertram et al., 2011). In addition, due to high sensitivity and

113 low detection limits, AMS has been successfully deployed at many remote sites with low aerosol mass

114 loading such as Antarctica (Schmale et al., 2013; Giordano et al., 2017). ~~However, there are not AMS~~

115 ~~measurement in the TP and Himalayas so far.~~

116

117 The study here presents ~~an analysis of comprehensive~~ results from measurements using an AMS ~~acquired~~

118 at the central ~~of the~~ TP during the transitional ~~season~~period from pre-monsoon to monsoon. The study was

119 designed to characterize aerosol chemical composition, temporal variations, transport processes, and

120 emission sources. During the campaign, besides the AMS, multiple other real-time instruments were also

121 deployed.

122

2. Methodology

2.1 Site description

125 The field study was conducted between May 31 and July 1, 2015 at a high altitude observatory, i.e., Nam

126 Co Station for Multisphere Observation and Research, Chinese Academy of Sciences (Nam Co station,

127 90°57′E, 30°46′N 4730m a.s.l), at the central part of the TP (Figure 1). The Nam Co station is located

128 nearby Nam Co lake (Figure 1b), the second largest inland lake in the TP (area: 1920 km^2) which is located

129 at the northern border of Nyainqentanglha Mountains. The melted glacier from Nyainqentanglha Mountains

130 supply water to the lake each year during warm seasons. ~~This~~The Nam Co station and its surrounding is a

131 pristine region except for a small county for local people that is about 10 km ~~to~~ west ~~of~~ to the station. In the

132 past several years, tourism for this beautiful lake has ~~growth.~~grown. A ~~highway~~freeway for tourists was

133 built about ~~1~~5 km south of the station. The capital city (Lhasa) of the Tibet Autonomous Region is about

134 100 km southeast of the station with an average elevation of 3600 m a.s.l. between which is

135 Nyainqentanglha Mountains (higher than 6000 m a.s.l) (Figure 1c). The closest town, Dangxiong, is

136 ~~along~~alongside the famous highway, Qinghai-Tibet Highway, and about 70 km east of the station with an

137 average elevation of 4200 m a.s.l. Overall, the station is ~~around~~surrounded by the mountains in the south

138 and east, and the lake at the west. The ecology of surrounding area is semi-arid ~~type~~ land dominated by

139 alpine meadow and barren areas. The precipitation is mainly occurred during summer monsoon period. The

140 cooking and heating at the station is ~~maintained~~supplied by the power and natural gas.

141

2.2 Instrument setup

143 The study was conducted at the observatory field of the station using a customer-made trailer with inlet

144 stepped out of the top with the height of ~5m above ground. All the instruments were arranged ~~in~~inside the

145 trailer where the air temperature ~~is~~was controlled at ~20°C by two ~~conditions. Figure 1 shows the set up of~~

146 ~~the instruments. The total~~air conditioners. The inlet was maintained by a vacuum pump with a flowrate of

147   10 ~~m/s~~L/min, following by a high-resolution time-of-flight aerosol mass spectrometer (HR-AMS,

148   Aerodyne Research Inc., Billerica, MA, USA), a custom-made scanning mobility particle sizer (SMPS), a

149   soot particle Aerodyne mass spectrometer (SP-AMS, Aerodyne Research Inc., Billerica, MA, USA), a

150   single-particle intracavity laser-induced incandescence photometer (SP2, DMT, Inc., Boulder, CO, USA),

151   and a seven wavelength Athelometer (model AE31, Magee Scientific, Berkeley, CA, USA). The total

152   flowrate of ~~this~~ the inlet was maintained at ~16 ~~m/s~~L/min and a $PM_{2.5}$ cyclone ~~at~~was used in the

153   ~~beginning~~front of the inlet (model URG-2000-30EH, URG Corp., Chapel Hill, NC, USA~~.~~) to remove

154   coarse particles. Several additional instruments were also co-located ~~but~~ with their own ~~inlet~~inlets, such as

155   a Nephelometer (model 3563, TSI, Shoreview, MN, USA), a $PM_{2.5}$ sampler (model PQ200, BGI, USA),

156   and a multi-angle absorption photometer (MAAP, model 5012, Thermo Electron Cooperation, USA). The

157   operations of the instruments used in this study were described below.

158

159   2.2.1 HR-AMS

160   HR-AMS was used to measure the non-refractory PM_1 ($NR\text{-}PM_1$~~)~~), which was ~~thermal~~thermally vaporized

161   at ~600 °C, ionized with a 70eV electron impact and ~~measured~~determined by using a time--of--flight mass

162   spectrometry. The details ~~on~~of the instrument have been described elsewhere (DeCarlo et al., 2006). For

163   ~~this~~our study, HR-AMS was only ~~setup~~operated with V-mode with 5 min resolution due to the low aerosol

164   mass loading. Due to ~~damage~~malfunction of the chopper,~~ the~~ size distribution of $NR\text{-}PM_1$ was not

165   determined. The HR-AMS was calibrated for ionization efficiency (IE) with the ammonium nitrate

166   following standard procedures (Jayne et al., 2000) at the beginning, in the middle and end of the study.

167   Particulate-free air was sampled ~~two times~~twice during the study period to adjust the ~~interaction~~influences

168   of air on the fragmentation table and determine the detection ~~limitation~~limits (DLs) of aerosol species. The

169   DLs were calculated as 3 times the standard deviations (3σ) of the measured values during ~~this period.~~the

170   particle-free sampling periods. The 2.5-min DLs for organic, sulfate, nitrate, ammonium, and chloride were

171   determined at 0.108, 0.014, 0.007, 0.002, 0.010 $\mu g\ m^{-3}$, which are comparable to the values reported in

172   previous studies.

173

174   2.2.2 Other instruments

175   The Aethalometer was used to measure the equivalent black carbon mass concentration using seven

176   wavelength lights. The data for BC is commonly calculated from measurement at 880 nm using

177   recommended MAC from ~~factory.~~the manufacture. The instrument was operated at the time resolution of 5

178   min with a flow rate of 5 L/min, which was calibrated ~~at~~once a week~~ frequency~~.

179

180    $PM_{2.5}$ sampler was ~~operated~~set up at the top of the trailer. Filter samples were collected between 2 June and

181   1 July 2015. Each aerosol sample was collected on a 47 mm quartz filter (Whatman, Maidstone, UK) using

182   the aerosol sampler~~.~~ with a flowrate of 16.7 L/min (BGI, USA, model PQ 200). The meteorological data

183   was recorded at the tower of the Nam Co station at a height of 20 m above ground.

184

2.3 Data processing

The HR-ToF-AMS data were processed using the standard software of SQUIRREL (v1.56) and PIKA (v1.15c) written in IGOR (Wavemetrics, Inc., Lake Oswego, OR, USA) (http://cires.colorado.edu/jimenez-group/ToFAMSResources/ToFSoftware/index.html) to determine the mass concentrations of the NR-PM$_1$ species and the ion-speciated mass spectra of organics~~, written in IGOR (Wavemetrics, Inc., Lake Oswego, OR, USA).~~. An empirical particle collection efficiency (CE) of 0.5 was used, which has been widely used in field studies employing AMS with a dryer installed in front of the equipment's particle inlet. This CE value was further validated by the consistency and reasonable slope between HR-AMS measured mass concentrations and SMPS-determined particle volumes (section 3.1.2, R^2 = 0.9, slope = 1.48). The elemental ratios of OA (O~:~/C, H~:~/C, and organic matter to carbon (OM~:~/OC)) ~~for~~in this study was determined using the "improved-ambient" method (Canagaratna et al., 2015). Default relative ionization efficiency (RIE) values were used for orgnaics (1.4), nitrate (1.1), and chloride (1.3), while an RIE value of 3.8 was determined for ammonium and 1.1 for sulfate based on the calibration for pure NH_4NO_3 and $(NH_4)_2SO_4$, respectively.

The source ~~decomposition~~apportionment of organics was ~~analysed~~conducted by PMF with the robust engine. First, organic matrix was analysed using the PMF2.exe algorithm in robust mode (Paatero and Tapper, 1994) and explored using the PMF Evaluation Toolkit (PET) (Ulbrich et al., 2009). The PMF solution was evaluated following the procedures outlined in Table 1 of ~~(Zhang et al., 2011) including modification of the error matrix and downweight of low S/N ions.~~Zhang et al. (2011) including modification of the error matrix and downweight of low signal-to-noise ions. Moreover, based on the AMS fragmentation table, some organic ions were not directly measured but scaled to the organic signal at m/z 44, which were downweighted by increasing their errors by a factor of 3. A two-factor solution with fPeak = 0 was chosen in this study, as it is able to reconstruct the total OA mass and temporal profiles very well. The results of three-factor solution with fPeak = 0 are shown in supplementary material (Figure S1), which show splitting ~~in~~of the solutions.

3 Results and discussions

3.1 The meteorological conditions during the study

During the field study, the meteorological conditions were generally cold and windy (Figure 2a and b). The average air temperature was 8.4 ± 3.6 °C with a diurnal hourly average ranging from 4.8 to 12.3 °C; the diurnal average wind speed (WS) ranged from 4.5 to 6.5 m s^{-1}. The dominant wind ~~direction was~~directions were south and southwest, although ~~it~~they varied during different periods (Figure 2b and S2). The wind direction (WD) had distinct diurnal variation with air mass from south during night to morning and west

during afternoon. Based on the report of the Climate Diagnostics Bulletin of India (http://imdpune.gov.in/Clim_RCC_LRF/Climate_Diagnostic_Bulletins/cdbi_apr_2015.pdf), the precipitation from Indian monsoon had covered most part of India on June 12 to June 14, and these days are treated as the onset of India monsoon. Indeed, precipitation was recorded at the Nam Co station on June 13 and lasted for several days (Figure 2a). Based on this weather condition, the period before June 14 was classified as the pre-monsoon period and afterwards as the monsoon period. The RH during the pre-monsoon and monsoon periods were $48.4 \pm 19.2\%$ and $58.8 \pm 16.5\%$, respectively. The ~~originations~~origins of the air masses were also different during these two periods. Figure 3 shows the air mass from west during pre-monsoon ~~periods~~period accounted about 30-40%, while it was only 7% during monsoon period, of which ~80% was from south.

3.2 The temporal ~~variation~~variations of chemical species

The average mass concentration of PM_1 (NR-PM_1 + BC) was 2.0 µg m^{-3} during the whole study period with 68% OA, 15% sulfate, 2% nitrate, 7% ammonium, and 8% BC. The NR-PM_1 mass loading (1.84 µg m^{-3}) at Nam Co Station was lower than the values observed at some high elevation sites such as Menyuan (10.8 µg m^{-3}) (Du et al., 2015), Montsec (4.9 µg m^{-3}) (Ripoll et al., 2015), Mt. Cimone (4.5 µg m^{-3}) (Rinaldi et al., 2015), Puy de Done (5 − 27 µg m^{-3}), and Mt. Bachelor (15.1 µg m^{-3}) (Zhou et al., 2017), but higher than those in some other sites, such as sub-Antarctic (0.46 µg m^{-3}) (Schmale et al., 2013) and Jungfraujoch (0.55 µg m^{-3}) (Fröhlich et al., 2015), similar with that at Mt. Whistler (1.91 µg m^{-3}) (Sun et al., 2009) (Table 1 and Figure S3). Although the sampling ~~season~~seasons and ~~elevation~~altitudes of these sampling sites are different (Table 1), the results of these studies could basically represent the level of pollution at these sits due to their relatively long sampling spans (from one month to ten months). The contribution of OA at these high-elevation sites ranged from 50% − 90%; the highest value was at Mt. Bachelor which was frequently influenced by transported biomass burning plume, while the relative low OA contribution (38%) at sub-Antarctic was due to the dominant source from marine emission containing ~~higher~~high sulfate. The mass concentration of PM_1 varied dynamically during ~~the~~our study with distinct difference between pre-monsoon and monsoon periods. The average mass concentrations of PM_1 for these two periods were 2.6 and 1.2 µg m^{-3}, respectively. For comparison, the ~~chemical~~concentrations of various species for these two periods were side-by-side displayed in Figure 4a. The ratios between pre-monsoon and monsoon for all the species were higher than 1 with the maxima for ammonium (3.1) and sulfate (2.8~~, suggesting high efficiency of wet scavenging for ammonium sulfate during monsoon. The~~); the contribution of OA was thus slightly higher during the monsoon period than during the pre-monsoon (71% vs. ~~64%).~~64% with a mass concentration ratio of 1.9). Apart from the potential scavenging effect, these results could also be influenced by the sources, transport route, and chemical processes during different periods.

257   Based on the mass concentration and temporal variations of PM_1 species and weather conditions, the pre-

258   monsoon period could be further divided into two periods, i.e., period 1 (P1: May 30 to June 7) and period

259   2 (P2: June 8 to June 13). ~~The~~ P1 was characterized by ~~higher~~relatively high sulfate concentration (0.46 vs.

260   0.41 µg m^{-3}) and sunny days, while P2 was characterized by ~~higher~~high PM_1 concentration (2.9 vs. 2.1 µg

261   m^{-3}~~), higher~~; P< 0.005, chi-square test), high nitrate contribution, and wet and cold days (Figure S4). The

262   air masses for P2 had higher contribution from west and north than those during P1 (Figure 3). Figure 4b

263   shows the comparisons of mass concentration of different species between these two periods. For chemical

264   species, from P1 to P2, nitrate and OA increased dramatically by a factor of 1.6 and 2.2, respectively, and

265   BC and ammonium ~~were~~ also increased, suggesting the influence of transported polluted air mass.

266   However, sulfate and chloride decreased slightly (the ratios between ~~P1~~P2 and ~~P2~~P1 were ~0.95). The

267   variations of sulfate and nitrate during these two periods could be related to the photochemical conditions

268   and origination of air mass (see section 3.3).

269

270   The particles were generally ~~chemical~~ neutralized as illustrated ~~from~~by the scatter plot between predicted

271   and measured ammonium (slope = 0.91) (Figure S5a). The neutralized PM_1 were likely due to the high

272   availability of ammonia from agriculture emission in North ~~of~~ India (Clarisse et al., 2009; Van Damme et

273   al., 2015). The slope was ~0.75 during P2 (Figure S5a), which suggested that there was ~~over~~excess

274   ammonium to neutralize sulfate and nitrate. We ~~check~~checked whether the high ~~concentration of~~

275   ammonium was from fragmentation of organic nitrogen such as ~~amine, however, the~~amines. The ratios of

276   NH^+ ~~and~~to NH_2^+ were consistently during the study (Figure S5b), suggesting there was no ~~amine~~significant

277   influences from amino compounds. This ~~high contribution from~~ excess ammonium determined by the

278   neutralization could be related to the presence of significant amounts of organic anions in aerosol (such as

279   carboxylic acids) or variation of RIE for ammonium which could have higher value in the mixed acidic

280   particles.

281

3.3 Diurnal variation and chemical process of different species

283

284   The diurnal ~~variation~~cycles of OA, sulfate, nitrate, ammonium, and BC during different periods are shown

285   in Figure 5. All these species ~~unexpected present significant diurnal patterns, especially during P2. The~~

286   ~~diurnal variation of aerosol are usually related to the local source emission (e.g., Xu et al., 2016). The~~

287   ~~diurnal variation at Nam Co may be related to the diurnal variations of long range transport air mass,~~

288   ~~photochemistry, and the variation of plenary boundary layer (PBL).~~unexpectedly present dramatic diurnal

289   variations, especially during P2. OA, sulfate, ammonium, and BC showed a similar pattern with low values

290   during nighttime to early morning and high values during afternoon. ~~We check~~ which suggest their

291   common sources or similar transport pathways (Zhang et al., 2001). We checked the diurnal variation of the

292   origination of air masses and found that there were increased air masses from south during nighttime and

293   from west during afternoon (Figure S6), which could be related to the plateau monsoon during summer

(Tang and Reiter, 1984). The enhanced air mass from west during afternoon could ~~be more favorable for transport~~favor the transportation of polluted air mass. The enhanced WS during afternoon was also observed with the increase of air temperature (Figure 5). The diurnal variations of chemical species during monsoon period were relatively flat comparing with those during P1 and P2~~.~~ which may relate with the relatively consistent air mass origination during monsoon. Nitrate presented a significant different diurnal variation with high values during nighttime to early morning and low values during afternoon. These features were highly correlated with that of the RH and air temperature (Figure 5) suggesting the ~~important chemical processing~~importance of thermodynamically-driven gas/particle~~/gas~~ partitioning of ammonium nitrate and heterogeneous production of nitrate due to hydrolysis of N_2O_5. In addition, during the early morning time (6:00 – 8:00), there ~~were~~was a peak for most ~~of~~species, which ~~were corresponding~~was accompanied with the lowest air temperature and the highest RH, ~~then~~and the lower plenary boundary layer (PBL), which could concentrate all the ~~polluted~~air ~~in a smaller space~~pollutants (Yanai and Li, 1994). Overall, the diurnal variations of aerosol species at Nam Co may be dominated by the variabilities of both long-range transport air mass and local meteorological conditions.

~~Although~~In order to further elucidate the ~~diurnal patterns for each species were similar during the three periods~~chemical processes and potential sources of the aerosol species, the relationships of chemical species with wind conditions were ~~significant different~~analyzed based on bivariate polar plot analysis (Figure 6). ~~Sulfate and ammonium during~~During P1~~.~~, sulfate and ammonium had hotspots from all ~~of the~~ directions ~~at~~across a ~~big~~wide range of wind speed (0 – 10 m s^{-1}~~) suggesting the local/regional transport and formation of ammonium sulfate from different air mass;~~); while OA ~~were concentrated depending to the~~was prevailing ~~wind direction~~from southeast and northwest ~~suggesting important transport routes for OA from these two directions~~winds; nitrate had hotspots ~~at~~when the ~~lowest~~wind speed was relatively slow (0 – 8 m s^{-1}) ~~only from southwest suggesting the nearby sources~~and~~/or local formation; while~~from southeast/east mainly; BC had hotspots from south, west and northwest at high wind ~~speed~~speeds (4 – 12 m s^{-1}~~) during P1 suggesting long range transport from the concentrated polluted regions in northern India and northwestern India.~~). During P2, all species except nitrate had hotspots from south/southwest at high wind ~~speed~~speeds (6 – 14 m s^{-1}~~), suggesting the different synoptic process comparing with that during P1.~~); Nitrate ~~still~~also had hotspots at a relative low wind speed from southwest ~~during P2~~. These results suggested that the sources and ~~chemical formation for~~formations of aerosols during P1 and P2 ~~were similar~~could be different, albeit the ~~wind conditions were different.~~diurnal variations of species between these two periods were similar. During monsoon period, all species had ~~more~~ similar ~~distribution~~distributions of the hotspots ~~and strongly~~, which could be from ~~northwest and weakly form~~all directions but relatively weak from southeast.

The significant difference of diurnal variation between sulfate and nitrate suggested the different chemical evolution of these two species. Nitrate and sulfate during three periods all had weak correlations. During P1,

the ratios of sulfate versus nitrate had peaks (> 20) during afternoon ~~time~~, while during P2, the ratios all kept at low values (< 20) (not shown). In order to further ~~check on~~investigate the chemical evolutions of these two species, we ~~dig out~~selected the high concentration periods based on nitrate concentration (> average + 2σ). Figure 7 showed all periods ~~during the~~with high nitrate ~~period of~~during the study and the corresponding meteorological conditions. It is easy to find that most of the high mass loading periods occurred during ~~the~~ nighttime. The wind speed and wind direction ~~were~~ varied dynamically and most of them were from southwest. Higher wind speed from this wind direction could transport more polluted air mass to Nam Co as illustrated from the event 1 (E1) during which all the species (OA, sulfate, ammonium, and BC) except nitrate increased; the weather during this type of event was accompanied with warm and dry air conditions. ~~While when~~When the wind direction was from southwest with lower wind speed (E2), the RH increased to higher than 90% accompanying with deceased air temperature, and the mass concentrations of nitrate, sulfate and OA increased significantly and BC decreased significantly in contrast ~~with~~to the increase of nitrate ~~being the most significant.~~. The decreased mass concentration of BC indicated no primary aerosol transportation, thus the increased species were mainly ~~secondary formation.~~secondarily formed.

3.4 The average chemical feature of organic aerosol

The average mass spectrum of OA was shown in Figure 8a. The organic mass was on average composed of 51% oxygen, 44% carbon, and 5% hydrogen with an average nominal formula being $C_1H_{1.33}O_{0.88}N_{0.001}$. On average, $C_xH_yO_1^+$ (38.1%) and $C_xH_y^+$ (37.3%) ions dominated the total OA following by $C_xH_yO_2^+$ (19.8%), and $H_yO_1^+$ (4.6%). m/z 44 was the base peak in the OA spectrum and mainly composed of CO_2^+ (99%). m/z 43 had ~~a significant contribution~~contributions from both $C_2H_3O^+$ (82%) and $C_3H_7^+$ (18%). m/z 55, likely an important primary fragment was consisted of 51% $C_4H_7^+$ and 49% $C_3H_3O^+$. The OA was highly oxidized with an O/C of 0.88 on average. The OA was more oxidized during pre-monsoon than monsoon with higher O ~~:~~/C ratio (0.~~90~~94 vs. 0.~~98~~72) and lower H ~~:~~/C ratio (1.~~30~~28 vs. 1.~~27~~44) (Figure 8b). The oxidation states of OA during two pre-monsoon periods were also different. The O/C during P2 (0.98) was higher than P1 (0.90) and the H/C was higher during P1 than P2~~.~~ (1.30 vs. 1.27). Correspondingly, the OA during P2 ~~was containing~~contained higher contribution of $C_xH_yO_1^+$ (40.3 vs. 39.1%) and $C_xH_yO_2^+$ (25.2 vs. 23.6%) ions than those ~~of~~during P1 (Figure 8c).

The diurnal variations of both O ~~:~~/C and OM ~~:~~/OC ratios presented higher values during late morning to afternoon and lower values during early morning (Figure 9a). H ~~:~~/C presented an opposite trend. These patterns suggested that OA was more oxidized during daytime which could be due to photo oxidation and/or transport of highly oxidized OA during daytime. We ~~check~~examined the variation of elemental ratios ~~at the function of~~ with OA mass concentrations, and found that the O ~~:~~/C ~~increased significantly~~increase was accompanied with the increase of OA mass concentration (Figure 9b). ~~This~~This

368 relationship could relate with the different influences of wet scavenging on more oxidized and less oxidized

369 OA. In addition, this result likely suggested the importance of transportation on the oxidized OA. during

370 afternoon due to the higher mass concentration occurring frequently on afternoon time. However it was not

371 possible that the polluted air mass arrived at Nam Co within several hours due to the long distance from

372 source regions (more than 1000 km from India). Previous studies have reported the presence of an aerosol

373 layer between 6 – 18 km a.s.l altitude over the Tibet Plateau during summer (Tobo et al., 2007; Vernier et

374 al., 2011). He et al. (2014) examined the vertical profiles of aerosol extinction coefficients measured with a

375 Micro Pulse Lidar at Naqu, about 100 km east of Nam Co Station, and observed a maximum in aerosol

376 extinction coefficient between 18 – 19 km a.s.l during summer 2011. Recently, Gu et al. (2016) examined

377 the chemicalaerosol compositions using the global three-dimensional Goddard Earth Observing System

378 chemical transport model (GEOS-Chem) and found elevated aerosol concentrations of sulfate, nitrate,

379 ammonium, BC, and organic carbon over the TP. Further, observational and modeling studies have also

380 shown that deep convection over the Tibet PlateauTP during daytime which is one of the important routes

381 for tropospheric and stratospheric exchange of aerosols (Cristofanelli et al., 2009; Cristofanelli et al., 2010;

382 Lin et al., 2016). Thus the enhanced aerosol concentrations during afternoon could possible frombe

383 possibly attributed to the mixed downward of aerosol layer at 16 – 18 km altitude during the growth of TP

384 boundary layer. This type of transportation could not be captured by the re-analysis of data used in the

385 back-trajectory analysis likely due to the low time and spatial resolution. The needNevertheless, this

386 hypothesis needs further validation in the future in this region.

3.5 The PMF decompositionapportionment on the OA

390 The two OA factors determined by PMF have distinctly different mass spectra and diurnal patterns (Figure

391 10), including a less oxidized OOA (LO-OOA; O:/C = 0.49) and a more oxidized OOA (MO-OOA; O:/C

392 = 0.96). Both factors appeared to be secondary in nature. Our inability to separate an HOAa primary traffic-

393 related OA factor is consistent with the fact that $C_4H_9^+$ was a minor peak in the OA spectra (0.6% of the

394 total signal) and the average organic-equivalent concentration of $C_4H_9^+$ was only 0.008 μg m^{-3} during this

395 study (Figure 5a). Collier et al. (2015) reported that the average $fC_4H_9^+$ (fraction of total organic signal

396 accounted for by $C_4H_9^+$) was 8.1% in the mass spectrum of POAprimary OA from vehicle emissions. Based

397 on this relationship, even assuming $C_4H_9^+$ was completely contributed by primary OA (POA) from vehicle

398 emissions-derived OA, the average HOAvehicle-OA concentration would be only ~ 0.1 ugμg m^{-3}, or 7% of

399 total OA mass, during thisour study. Note that in this study, $C_4H_9^+$ was fitfitted well in the PMF analysis

400 with very small residual, indicating that the signal of this ion was properly apportioned between the two

401 OOA factors.

403 The mass spectra of MO-OOA and LO-OOA were characterized by high peaks at m/z 44 (mostly CO_2^+)

404 and LO-OOA had a relative large peak at m/z 43 (mostly $C_2H_3O^+$) as well (Figure 10a). The contributions

of the $C_xH_yO_2^+$ ion category in these two mass spectra were 15.1% and 28.6%, respectively, while the

contributions of $C_xH_yO_1^+$ were 37.8% and 41.5%, respectively. The time series of LO-OOA correlated well

with $C_xH_yO_1^+$ and $C_xH_y^+$ ions, while MO-OOA correlated well with $C_xH_yO_2^+$ ions (Figure S7). In addition,

the time series of MO-OOA correlated well with sulfate ($R^2 = 0.55$), BC ($R^2 = 0.54$) and less well with

nitrate ($R^2 = 0.33$), while LO-OOA correlated poorly with sulfate, BC and nitrate (Figure 10b and S8).

These results highlight the oxidation degree of MO-OOA and LO-OOA. LO-OOA and MO-OOA

accounted for 41% and 59% on average, respectively, of total OA mass during this study (Figure 11a), and

their relative contributions varied across the study (Figure 2e). For example, LO-OOA accounted for 41%

of the total OA mass during P1 ~~of the pre-monsoon period~~, 24% during P2, and 67% during the monsoon

period (Figure 11b). The diurnal pattern of MO-OOA was characterized by higher concentrations during

afternoon similar to those of sulfate and BC. While the diurnal pattern of LO-OOA peaked at early evening

time (Figure 10c). The polar plot showed concentrated hotspots to the northwest of the sampling site for

MO-OOA, and southeast for LO-OOA (Figure 6), indicating that the sources of these two components were

totally different. MO-OOA was likely closely related to long-range transport of air mass from South Asia,

while LO-OOA could from relative shorter distance transport such as marine air mass and regional

background aerosol during the nighttime. Shen et al. (2015) reported that there were significant aerosol

source from biogenic emission during summer near the Nam Co Station. As shown in Figure 12a and b,

MO-OOA, which was highly oxidized (O~:~/C = 0.96), appeared on the up-left corner of the triangle plot

while LO-OOA was in the middle part with an O~:~/C ratio of 0.49. The high oxidation degree of MO-OOA

was likely related to extensive aging processes occurred during long-range transport. The slope of linear

fitting of all the data points in V-K diaphragm is –0.76 suggesting the evolution of OA as carboxylic acid

functionalization (Figure 12c).

Biomass burning emission is an important source in South Asia and could be transported to Himalayas and

TP during pre-monsoon (Engling et al., 2011; Kumar et al., 2011; Sang et al., 2013; Cong et al., 2015),

however there are not ~~evidently~~significant signals of biomass ~~emitted~~burning aerosol in our AMS results

such as signals at m/z 60 and 73 in mass spectrum of OA which were found to be associated with

levoglucosan formed from the pyrolysis of cellulose (Alfarra et al., 2007). The contribution of *f*60 (fraction

of total organic signal accounted for by m/z 60) for LO-OOA and MO-OOA were 0.2% and 0.3%,

respectively, which were similar with the global background level (less than 0.3%) suggested by Cubison et

al. (2011). These results suggest that OA, if ever partly originated from biomass burning emission, could

have been highly oxidized during transport. This behavior had been observed in a few studies that

levoglucosan could be quickly (within a few hours) oxidized after being emitted (Ortega et al., 2013). In

addition, Zhou et al. (2017) recently reported the observation of a highly aged BBOA factor with *f60 < 0.3%*

in its mass spectrum, in aged wildfire plumes that had gone through extensive photochemical oxidation.

3.6 Sensitivity of the ~~chemical characteristics~~transport of ~~PM₁~~pollutants to synoptic process

Synoptic process is an important factor determining if the regional emissions can be transported to the TP. It is interesting to know what kind of synoptic process is favorable for transporting the polluted air mass to the Himalayas and the TP. A 3-D Regional chemical transport Model (REAM) coupled with the Weather Research and Forecasting model (WRF) was used to examine the chemical evolution and regional transport of pollutants such as aromatics in this study. REAM has been used in previous studies of the Tibet Plateau, and details about the model can be found in ~~Zhang et al. (2017)~~Zhang et al. (2017) and supplementary material. REAM could capture some synoptic processes which cannot be simulated by the normally used reanalysis data due to their low-resolution and the complexity of terrain in the Tibet Plateau ~~(Zhang et al., 2017)~~(Zhang et al., 2017). Figure 13 shows the distribution of simulated daily surface wind, 300 hPa geopotential height fields and concentrations of reactive aromatics over the Tibetan Plateau during 30 May – 13 June, 2015. During 30 May to 7 June corresponding to P1 ~~in this study~~, there was a trough over the north propagated from west to east and this low pressure induced increasingly stronger surface wind from India to the TP, which could lead to transport of polluted air mass as illustrated by the results of model and AMS. The simulated concentration of reactive aromatics showed a peak during this period (Figure S9). During 8-11 June, there was a weak ridge system over the north. Intensified wind from north was observed as illustrated by HYSPLIT results (Figure 5b) and the simulated concentrations of reactive aromatics were sharply decreased (Figure S9). After that, a weak low-pressure trough system was observed again. The increased concentrations of reactive aromatics were also observed accompanying with intensified southern wind. ~~These~~Although these trends ~~were~~ are basically consistent with ~~that~~our AMS results~~.~~, there were also significant differences (Figure S9). The ~~potential~~possible reason ~~for this difference~~ was that the weak trough during P2 intensified the wind from west other than south where a lot of biomass burning emission sources ~~were located (Figure 5b). Meanwhile the interaction between cold dry air mass from north and warm wet air mass from south increased the RH at Nam Co which was very favorable for aqueous formation.~~locate (Figure 5b). Zhang et al., (2017) suggested that a low-cut system from stratosphere could be an important driver for pollution transport into the ~~Tibet Plateau. However,~~TP. In our study, the trough/ridge system seems to be also an important factor affecting the transport of air pollution from south and west, although this effect tends to be weaker in summer than in the other seasons because the tropopause is higher and stratospheric wave activity is weaker in summer. ~~In our study, the trough/ridge system could be an important factor affecting on the transport of air pollution from south and west.~~

3.7 Atmospheric implications

Our results have several potential implications to the atmospheric studies in the TP and Himalayas. Firstly, it is useful for the accurate estimation of the radiative forcing of aerosols in this region and validation of

current model simulation results based on our observed chemical composition and mass loadings of fine aerosols. Ji et al. (2015) estimate the radiative forcing from aerosols over the TP and Himalayas at the surface level using a regional climate model (RegCM4.3); for carbonaceous aerosols, there are several literatures that tested the model results, but all other species were referred to data available in the published inventory with a coarse spatial resolution. Secondly, our findings are implicate to the estimation of aerosol deposition on the glacier of this region and evaluation of subsequent impacts on the melting of snow/ice (Yasunari et al., 2010). Thirdly, highly-time resolved aerosol data is very scarce in this remote plateau, thus our data are valuable to validate modeling results regarding the transport of polluted air mass as demonstrated in section 3.6. At last, the transport mechanism of aerosol to the inland of TP is less understood so far. Hindman and Upadhyay (2002) suggested that the vertical lifting due to convection and subsequent horizontal mountain-valley wind could lead to the transport of aerosol from Nepal to Tibet. Dumka et al. (2010) also highlighted the important role of mountain-valley wind in the aerosol transport in the central Himalayas. The dynamic variations of aerosol chemical species measured here, are likely helpful to elucidate the transport mechanism of polluted air mass. Nevertheless, this scientific issue required further detailed investigations in the future.

4. Conclusion

The average PM_1 loading measured at Nam Co during June 2015 was 2.0 $\mu g\ m^{-3}$ with organics accounting for 68%, followed by sulfate (15%), black carbon (8%), ammonium (7%), and nitrate (2%). This mass concentration was comparable to some AMS observations from mountain-top sites. The mass concentration of PM_1 varied during different weather conditions with higher concentration during pre-monsoon and lower concentration during monsoon. The pre-monsoon period could also be divided into two periods (P1 and P2) based on meteorological conditions and aerosol chemical composition. During P1, PM_1 was characterized with high contribution from OA and sulfate, while increased contribution of nitrate was observed during P2 with wet and cold weather conditions. All PM_1 species had clear diurnal variations with OA, sulfate, BC, and ammonium peaking during afternoon due to photochemical production of these species coupled with transport of polluted air mass. Nitrate, however, peaked during the nighttime and early morning, which was related to the ~~higher~~high RH condition~~.~~ and low air temperature. The formation of nitrate was highly correlated with transport of air masses from southwest under very low wind speeds, while the mass concentrations of sulfate, OA, and BC were highly correlated with air masses from northwest and southeast under higher wind speed conditions. OA was overall highly oxidized during the entire study with higher O/C ratios during the pre-monsoon period. Based on PMF analysis, the OA was found to be composed of a LO-OOA and a MO-OOA. LO-OOA was mainly associated with air masses originated from south, while MO-OOA was mainly from northwest. MO-OOA dominated OA during the pre-monsoon period, while LO-OOA dominated during the monsoon period. The transport mechanism of polluted air plume was further ~~checked~~investigated by using the REAM chemical model coupled with the WRF model. The

515 polluted air plume was found to be more easily transported to the TP and Himalayas during low pressure
516 trough weather.
517

Acknowledgements

519

520 Thanks for the logistical supports of Nam Co Station for Multisphere Observation and Research, Chinese
521 Academy of Sciences. This research was supported by grants from the ~~Key Laboratory of Cryospheric~~
522 ~~Sciences Scientific Research Foundation (SKLCS-ZZ-2017-01), the~~ National Natural Science Foundation
523 of China (41771079, 41330526), the National Natural Science Foundation of China Science Fund for
524 Creative Research Groups (41421061), the Key Laboratory of Cryospheric Sciences Scientific Research
525 Foundation (SKLCS-ZZ-2017-01), the US National Science Foundation, and the Chinese Academy of
526 Sciences Hundred Talents Program.

Reference:

Aiken, A. C., DeCarlo, P. F., Kroll, J. H., Worsnop, D. R., Huffman, J. A., Docherty, K. S., Ulbrich, I. M., Mohr, C., Kimmel, J. R., Sueper, D., Sun, Y., Zhang, Q., Trimborn, A., Northway, M., Ziemann, P. J., Canagaratna, M. R., Onasch, T. B., Alfarra, M. R., Prevot, A. S. H., Dommen, J., Duplissy, J., Metzger, A., Baltensperger, U., and Jimenez, J. L.: O/C and OM/OC Ratios of Primary, Secondary, and Ambient Organic Aerosols with High-Resolution Time-of-Flight Aerosol Mass Spectrometry, Environ. Sci. Technol., 42, 4478-4485, 10.1021/es703009q, 2008.

Alfarra, M. R., Prevot, A. S. H., Szidat, S., Sandradewi, J., Weimer, S., Lanz, V. A., Schreiber, D., Mohr, M., and Baltensperger, U.: Identification of the Mass Spectral Signature of Organic Aerosols from Wood Burning Emissions, Environ. Sci. Technol., 41, 5770-5777, 10.1021/es062289b, 2007.

Bertram, A., Martin, S., Hanna, S., Smith, M., Bodsworth, A., Chen, Q., Kuwata, M., Liu, A., You, Y., and Zorn, S.: Predicting the relative humidities of liquid-liquid phase separation, efflorescence, and deliquescence of mixed particles of ammonium sulfate, organic material, and water using the organic-to-sulfate mass ratio of the particle and the oxygen-to-carbon elemental ratio of the organic component, Atmos. Chem. Phys., 11, 10995-11006, 10.5194/acp-11-10995-2011, 2011.

Bonasoni, P., Laj, P., Marinoni, A., Sprenger, M., Angelini, F., Arduini, J., Bonafè, U., Calzolari, F., Colombo, T., Decesari, S., Di Biagio, C., di Sarra, A. G., Evangelisti, F., Duchi, R., Facchini, M. C., Fuzzi, S., Gobbi, G. P., Maione, M., Panday, A., Roccato, F., Sellegri, K., Venzac, H., Verza, G. P., Villani, P., Vuillermoz, E., and Cristofanelli, P.: Atmospheric Brown Clouds in the Himalayas: first two years of continuous observations at the Nepal Climate Observatory-Pyramid (5079 m), Atmos. Chem. Phys., 10, 7515-7531, 10.5194/acp-10-7515-2010, 2010.

Canagaratna, M. R., Jayne, J. T., Jimenez, J. L., Allan, J. D., Alfarra, M. R., Zhang, Q., Onasch, T. B., Drewnick, F., Coe, H., Middlebrook, A., Delia, A., Williams, L. R., Trimborn, A. M., Northway, M. J., DeCarlo, P. F., Kolb, C. E., Davidovits, P., and Worsnop, D. R.: Chemical and microphysical characterization of ambient aerosols with the aerodyne aerosol mass spectrometer, Mass. Spectrom. Rev., 26, 185-222, 10.1002/mas.20115, 2007.

Canagaratna, M. R., Jimenez, J. L., Kroll, J. H., Chen, Q., Kessler, S. H., Massoli, P., Hildebrandt Ruiz, L., Fortner, E., Williams, L. R., Wilson, K. R., Surratt, J. D., Donahue, N. M., Jayne, J. T., and Worsnop, D. R.: Elemental ratio measurements of organic compounds using aerosol mass spectrometry: characterization, improved calibration, and implications, Atmos. Chem. Phys., 15, 253-272, 10.5194/acp-15-253-2015, 2015.

Clarisse, L., Clerbaux, C., Dentener, F., Hurtmans, D., and Coheur, P.-F.: Global ammonia distribution derived from infrared satellite observations, Nature Geosci., 2, 479-483, 10.1038/ngeo551, 2009.

Collier, S., Zhou, S., Kuwayama, T., Forestieri, S., Brady, J., Zhang, M., Kleeman, M., Cappa, C., Bertram, T., and Zhang, Q.: Organic PM Emissions from Vehicles: Composition, O/C Ratio, and Dependence on PM Concentration, Aerosol. Sci. Tech., 49, 86-97, 10.1080/02786826.2014.1003364, 2015.

Cong, Z., Kang, S., Kawamura, K., Liu, B., Wan, X., Wang, Z., Gao, S., and Fu, P.: Carbonaceous aerosols on the south edge of the Tibetan Plateau: concentrations, seasonality and sources, Atmos. Chem. Phys., 15, 1573-1584, 10.5194/acp-15-1573-2015, 2015.

Cristofanelli, P., Bonasoni, P., Bonafé, U., Calzolari, F., Duchi, R., Marinoni, A., Roccato, F., Vuillermoz, E., and Sprenger, M.: Influence of lower stratosphere/upper troposphere transport events on surface ozone at the Everest-Pyramid GAW Station (Nepal): first year of analysis, International Journal of Remote Sensing, 30, 4083-4097, 10.1080/01431160902821940, 2009.

Cristofanelli, P., Bracci, A., Sprenger, M., Marinoni, A., Bonafè, U., Calzolari, F., Duchi, R., Laj, P., Pichon, J. M., Roccato, F., Venzac, H., Vuillermoz, E., and Bonasoni, P.: Tropospheric ozone variations at the Nepal Climate Observatory-Pyramid (Himalayas, 5079 m a.s.l.) and influence of deep stratospheric intrusion events, Atmos. Chem. Phys., 10, 6537-6549, 10.5194/acp-10-6537-2010, 2010.

Cubison, M. J., Ortega, A. M., Hayes, P. L., Farmer, D. K., Day, D., Lechner, M. J., Brune, W. H., Apel, E., Diskin, G. S., Fisher, J. A., Fuelberg, H. E., Hecobian, A., Knapp, D. J., Mikoviny, T., Riemer, D., Sachse, G. W., Sessions, W., Weber, R. J., Weinheimer, A. J., Wisthaler, A., and Jimenez, J. L.: Effects of aging on organic aerosol from open biomass burning smoke in aircraft and laboratory studies, Atmos. Chem. Phys., 11, 12049-12064, 10.5194/acp-11-12049-2011, 2011.

581 DeCarlo, P. F., Kimmel, J. R., Trimborn, A., Northway, M. J., Jayne, J. T., Aiken, A. C., Gonin, M., Fuhrer,
582   K., Horvath, T., Docherty, K. S., Worsnop, D. R., and Jimenez, J. L.: Field-Deployable, High-
583   Resolution, Time-of-Flight Aerosol Mass Spectrometer, Anal. Chem., 78, 8281-8289,
584   10.1021/ac061249n, 2006.
585 Du, W., Sun, Y. L., Xu, Y. S., Jiang, Q., Wang, Q. Q., Yang, W., Wang, F., Bai, Z. P., Zhao, X. D., and
586   Yang, Y. C.: Chemical characterization of submicron aerosol and particle growth events at a
587   national background site (3295 m a.s.l.) on the Tibetan Plateau, Atmos. Chem. Phys., 15, 10811-
588   10824, 10.5194/acp-15-10811-2015, 2015.
589 Dumka, U. C., Moorthy, K. K., Kumar, R., Hegde, P., Sagar, R., Pant, P., Singh, N., and Babu, S. S.:
590   Characteristics of aerosol black carbon mass concentration over a high altitude location in the
591   Central Himalayas from multi-year measurements, Atmos. Res., 96, 510-521,
592   10.1016/j.atmosres.2009.12.010, 2010.
593 Engling, G., Zhang, Y.-N., Chan, C.-Y., Sang, X.-F., Lin, M., Ho, K.-F., Li, Y.-S., Lin, C.-Y., and Lee, J. J.:
594   Characterization and sources of aerosol particles over the southeastern Tibetan Plateau during the
595   Southeast Asia biomass-burning season, Tellus. B, 63, 117-128, 10.1111/j.1600-
596   0889.2010.00512.x, 2011.
597 Fang, K., Makkonen, R., Guo, Z., Zhao, Y., and Seppa, H.: An increase in the biogenic aerosol
598   concentration as a contributing factor to the recent wetting trend in Tibetan Plateau, Scientific
599   Reports, 5, 10.1038/srep14628, 2015.
600 Freney, E. J., Sellegri, K., Canonaco, F., Boulon, J., Hervo, M., Weigel, R., Pichon, J. M., Colomb, A.,
601   Prévôt, A. S. H., and Laj, P.: Seasonal variations in aerosol particle composition at the puy-de-
602   Dôme research station in France, Atmos. Chem. Phys., 11, 13047-13059, 10.5194/acp-11-13047-
603   2011, 2011.
604 Fröhlich, R., Crenn, V., Setyan, A., Belis, C. A., Canonaco, F., Favez, O., Riffault, V., Slowik, J. G., Aas,
605   W., Aijälä, M., Alastuey, A., Artiñano, B., Bonnaire, N., Bozzetti, C., Bressi, M., Carbone, C.,
606   Coz, E., Croteau, P. L., Cubison, M. J., Esser-Gietl, J. K., Green, D. C., Gros, V., Heikkinen, L.,
607   Herrmann, H., Jayne, J. T., Lunder, C. R., Minguillón, M. C., Močnik, G., O'Dowd, C. D.,
608   Ovadnevaite, J., Petralia, E., Poulain, L., Priestman, M., Ripoll, A., Sarda-Estève, R.,
609   Wiedensohler, A., Baltensperger, U., Sciare, J., and Prévôt, A. S. H.: ACTRIS ACSM
610   intercomparison – Part 2: Intercomparison of ME-2 organic source apportionment results from 15
611   individual, co-located aerosol mass spectrometers, Atmos. Meas. Tech., 8, 2555-2576,
612   10.5194/amt-8-2555-2015, 2015.
613 Giordano, M. R., Kalnajs, L. E., Avery, A., Goetz, J. D., Davis, S. M., and DeCarlo, P. F.: A missing
614   source of aerosols in Antarctica – beyond long-range transport, phytoplankton, and
615   photochemistry, Atmos. Chem. Phys., 17, 1-20, 10.5194/acp-17-1-2017, 2017.
616 Gu, Y., Liao, H., and Bian, J.: Summertime nitrate aerosol in the upper troposphere and lower stratosphere
617   over the Tibetan Plateau and the South Asian summer monsoon region, Atmos. Chem. Phys., 16,
618   6641-6663, 10.5194/acp-16-6641-2016, 2016.
619 He, Q. S., Li, C. C., Ma, J. Z., Wang, H. Q., Yan, X. L., Lu, J., Liang, Z. R., and Qi, G. M.: Lidar-observed
620   enhancement of aerosols in the upper troposphere and lower stratosphere over the Tibetan Plateau
621   induced by the Nabro volcano eruption, Atmos. Chem. Phys., 14, 11687-11696, 10.5194/acp-14-
622   11687-2014, 2014.
623 Heald, C. L., Kroll, J. H., Jimenez, J. L., Docherty, K. S., DeCarlo, P. F., Aiken, A. C., Chen, Q., Martin, S.
624   T., Farmer, D. K., and Artaxo, P.: A simplified description of the evolution of organic aerosol
625   composition in the atmosphere, Geophys. Res. Lett., 37, L08803, 10.1029/2010gl042737, 2010.
626 Hindman, E. E., and Upadhyay, B. P.: Air pollution transport in the Himalayas of Nepal and Tibet during
627   the 1995-1996 dry season, Atmospheric Environment, 36, 727-739, Doi 10.1016/S1352-
628   2310(01)00495-2, 2002.
629 Jayne, J. T., Leard, D. C., Zhang, X., Davidovits, P., Smith, K. A., Kolb, C. E., and Worsnop, D. R.:
630   Development of an Aerosol Mass Spectrometer for Size and Composition Analysis of Submicron
631   Particles, Aerosol. Sci. Tech., 33, 49 - 70, http://dx.doi.org/10.1080/027868200410840, 2000.
632 Ji, Z. M., Kang, S. C., Cong, Z. Y., Zhang, Q. G., and Yao, T. D.: Simulation of carbonaceous aerosols
633   over the Third Pole and adjacent regions: distribution, transportation, deposition, and climatic
634   effects, Climate Dynamics, 45, 2831-2846, 2015.
635 Jimenez, J. L., Canagaratna, M. R., Donahue, N. M., Prevot, A. S. H., Zhang, Q., Kroll, J. H., DeCarlo, P.
636   F., Allan, J. D., Coe, H., Ng, N. L., Aiken, A. C., Docherty, K. S., Ulbrich, I. M., Grieshop, A. P.,

Robinson, A. L., Duplissy, J., Smith, J. D., Wilson, K. R., Lanz, V. A., Hueglin, C., Sun, Y. L., Tian, J., Laaksonen, A., Raatikainen, T., Rautiainen, J., Vaattovaara, P., Ehn, M., Kulmala, M., Tomlinson, J. M., Collins, D. R., Cubison, M. J., E., Dunlea, J., Huffman, J. A., Onasch, T. B., Alfarra, M. R., Williams, P. I., Bower, K., Kondo, Y., Schneider, J., Drewnick, F., Borrmann, S., Weimer, S., Demerjian, K., Salcedo, D., Cottrell, L., Griffin, R., Takami, A., Miyoshi, T., Hatakeyama, S., Shimono, A., Sun, J. Y., Zhang, Y. M., Dzepina, K., Kimmel, J. R., Sueper, D., Jayne, J. T., Herndon, S. C., Trimborn, A. M., Williams, L. R., Wood, E. C., Middlebrook, A. M., Kolb, C. E., Baltensperger, U., and Worsnop, D. R.: Evolution of Organic Aerosols in the Atmosphere, Science, 326, 1525-1529, 10.1126/science.1180353, 2009.

Kroll, J. H., Donahue, N. M., Jimenez, J. L., Kessler, S. H., Canagaratna, M. R., Wilson, K. R., Altieri, K. E., Mazzoleni, L. R., Wozniak, A. S., Bluhm, H., Mysak, E. R., Smith, J. D., Kolb, C. E., and Worsnop, D. R.: Carbon oxidation state as a metric for describing the chemistry of atmospheric organic aerosol, Nature Chem., 3, 133-139, 10.1038/nchem.948, 2011.

Kumar, R., Naja, M., Satheesh, S. K., Ojha, N., Joshi, H., Sarangi, T., Pant, P., Dumka, U. C., Hegde, P., and Venkataramani, S.: Influences of the springtime northern Indian biomass burning over the central Himalayas, J. Geophys. Res.-Atmos., 116, 10.1029/2010jd015509, 2011.

Li, Z., Lau, W. K. M., Ramanathan, V., Wu, G., Ding, Y., Manoj, M. G., Liu, J., Qian, Y., Li, J., Zhou, T., Fan, J., Rosenfeld, D., Ming, Y., Wang, Y., Huang, J., Wang, B., Xu, X., Lee, S. S., Cribb, M., Zhang, F., Yang, X., Zhao, C., Takemura, T., Wang, K., Xia, X., Yin, Y., Zhang, H., Guo, J., Zhai, P. M., Sugimoto, N., Babu, S. S., and Brasseur, G. P.: Aerosol and monsoon climate interactions over Asia, Rev. Geophys., 54, 2015RG000500, 10.1002/2015RG000500, 2016.

Lin, M., Zhang, Z., Su, L., Hill-Falkenthal, J., Priyadarshi, A., Zhang, Q., Zhang, G., Kang, S., Chan, C.-Y., and Thiemens, M. H.: Resolving the impact of stratosphere-to-troposphere transport on the sulfur cycle and surface ozone over the Tibetan Plateau using a cosmogenic 35S tracer, Journal of Geophysical Research: Atmospheres, 121, 2015JD023801, 10.1002/2015JD023801, 2016.

Liu, B., Cong, Z., Wang, Y., Xin, J., Wan, X., Pan, Y., Liu, Z., Wang, Y., Zhang, G., Wang, Z., Wang, Y., and Kang, S.: Background aerosol over the Himalayas and Tibetan Plateau: observed characteristics of aerosol mass loading, Atmos. Chem. Phys., 17, 449-463, 10.5194/acp-17-449-2017, 2017.

Lu, Z., Streets, D. G., Zhang, Q., and Wang, S.: A novel back-trajectory analysis of the origin of black carbon transported to the Himalayas and Tibetan Plateau during 1996–2010, Geophys. Res. Lett., 39, L01809, 10.1029/2011gl049903, 2012.

Lüthi, Z. L., Škerlak, B., Kim, S. W., Lauer, A., Mues, A., Rupakheti, M., and Kang, S.: Atmospheric brown clouds reach the Tibetan Plateau by crossing the Himalayas, Atmos. Chem. Phys., 15, 6007-6021, 10.5194/acp-15-6007-2015, 2015.

Marinoni, A., Cristofanelli, P., Laj, P., Duchi, R., Calzolari, F., Decesari, S., Sellegri, K., Vuillermoz, E., Verza, G. P., Villani, P., and Bonasoni, P.: Aerosol mass and black carbon concentrations, a two year record at NCO-P (5079 m, Southern Himalayas), Atmos. Chem. Phys., 10, 8551-8562, 10.5194/acp-10-8551-2010, 2010.

Marinoni, A., Cristofanelli, P., Laj, P., Duchi, R., Putero, D., Calzolari, F., Landi, T. C., Vuillermoz, E., Maione, M., and Bonasoni, P.: High black carbon and ozone concentrations during pollution transport in the Himalayas: Five years of continuous observations at NCO-P global GAW station, Journal of Environmental Sciences, 25, 1618-1625, 10.1016/s1001-0742(12)60242-3, 2013.

Ng, N. L., Canagaratna, M. R., Jimenez, J. L., Chhabra, P. S., Seinfeld, J. H., and Worsnop, D. R.: Changes in organic aerosol composition with aging inferred from aerosol mass spectra, Atmos. Chem. Phys. Discuss., 11, 7095-7112, 10.5194/acpd-11-7095-2011, 2011.

Ortega, A. M., Day, D. A., Cubison, M. J., Brune, W. H., Bon, D., de Gouw, J. A., and Jimenez, J. L.: Secondary organic aerosol formation and primary organic aerosol oxidation from biomass-burning smoke in a flow reactor during FLAME-3, Atmos. Chem. Phys., 13, 11551-11571, 10.5194/acp-13-11551-2013, 2013.

Paatero, P., and Tapper, U.: Positive matrix factorization: A non-negative factor model with optimal utilization of error estimates of data values, Environmetrics, 5, 111-126, 10.1002/env.3170050203, 1994.

Rinaldi, M., Gilardoni, S., Paglione, M., Sandrini, S., Fuzzi, S., Massoli, P., Bonasoni, P., Cristofanelli, P., Marinoni, A., Poluzzi, V., and Decesari, S.: Organic aerosol evolution and transport observed at

Mt. Cimone (2165 m a.s.l.), Italy, during the PEGASOS campaign, Atmos. Chem. Phys., 15, 11327-11340, 10.5194/acp-15-11327-2015, 2015.

Ripoll, A., Minguillón, M. C., Pey, J., Jimenez, J. L., Day, D. A., Sosedova, Y., Canonaco, F., Prévôt, A. S. H., Querol, X., and Alastuey, A.: Long-term real-time chemical characterization of submicron aerosols at Montsec (southern Pyrenees, 1570 m a.s.l.), Atmos. Chem. Phys., 15, 2935-2951, 10.5194/acp-15-2935-2015, 2015.

Sang, X., Zhang, Z., Chan, C., and Engling, G.: Source categories and contribution of biomass smoke to organic aerosol over the southeastern Tibetan Plateau, Atmospheric Environment, 78, 113-123, 10.1016/j.atmosenv.2012.12.012, 2013.

Schmale, J., Schneider, J., Nemitz, E., Tang, Y. S., Dragosits, U., Blackall, T. D., Trathan, P. N., Phillips, G. J., Sutton, M., and Braban, C. F.: Sub-Antarctic marine aerosol: dominant contributions from biogenic sources, Atmos. Chem. Phys., 13, 8669-8694, 10.5194/acp-13-8669-2013, 2013.

Shen, R. Q., Ding, X., He, Q. F., Cong, Z. Y., Yu, Q. Q., and Wang, X. M.: Seasonal variation of secondary organic aerosol tracers in Central Tibetan Plateau, Atmos. Chem. Phys., 15, 8781-8793, 10.5194/acp-15-8781-2015, 2015.

Stockwell, C. E., Christian, T. J., Goetz, J. D., Jayarathne, T., Bhave, P. V., Praveen, P. S., Adhikari, S., Maharjan, R., DeCarlo, P. F., Stone, E. A., Saikawa, E., Blake, D. R., Simpson, I. J., Yokelson, R. J., and Panday, A. K.: Nepal Ambient Monitoring and Source Testing Experiment (NAMaSTE): emissions of trace gases and light-absorbing carbon from wood and dung cooking fires, garbage and crop residue burning, brick kilns, and other sources, Atmos. Chem. Phys., 16, 11043-11081, 10.5194/acp-16-11043-2016, 2016.

Stone, E. A., Schauer, J. J., Pradhan, B. B., Dangol, P. M., Habib, G., Venkataraman, C., and Ramanathan, V.: Characterization of emissions from South Asian biofuels and application to source apportionment of carbonaceous aerosol in the Himalayas, J. Geophys. Res.-Atmos., 115, 10.1029/2009jd011881, 2010.

Sun, Y., Zhang, Q., Macdonald, A. M., Hayden, K., Li, S. M., Liggio, J., Liu, P. S. K., Anlauf, K. G., Leaitch, W. R., Steffen, A., Cubison, M., Worsnop, D. R., van Donkelaar, A., and Martin, R. V.: Size-resolved aerosol chemistry on Whistler Mountain, Canada with a high-resolution aerosol mass spectrometer during INTEX-B, Atmos. Chem. Phys., 9, 3095-3111, 10.5194/acp-9-3095-2009, 2009.

Tang, M., and Reiter, E. R.: Plateau monsoons of the Northern Hemisphere: A comparison between North America and Tibet, Monthly Weather Review, 112, 617-637, 1984.

Tobo, Y., Zhang, D., Iwasaka, Y., and Shi, G.: On the mixture of aerosols and ice clouds over the Tibetan Plateau: Results of a balloon flight in the summer of 1999, Geophys. Res. Lett., 34, L23801, 10.1029/2007GL031132, 2007.

Ulbrich, I. M., Canagaratna, M. R., Zhang, Q., Worsnop, D. R., and Jimenez, J. L.: Interpretation of organic components from Positive Matrix Factorization of aerosol mass spectrometric data, Atmos. Chem. Phys., 9, 2891-2918, 10.5194/acp-9-2891-2009, 2009.

Van Damme, M., Erisman, J. W., Clarisse, L., Dammers, E., Whitburn, S., Clerbaux, C., Dolman, A. J., and Coheur, P. F.: Worldwide spatiotemporal atmospheric ammonia (NH3) columns variability revealed by satellite, Geophys. Res. Lett., 42, 8660-8668, 2015.

Vernier, J. P., Thomason, L. W., and Kar, J.: CALIPSO detection of an Asian tropopause aerosol layer, Geophys. Res. Lett., 38, L07804, 10.1029/2010GL046614, 2011.

Xu, C., Ma, Y. M., Panday, A., Cong, Z. Y., Yang, K., Zhu, Z. K., Wang, J. M., Amatya, P. M., and Zhao, L.: Similarities and differences of aerosol optical properties between southern and northern sides of the Himalayas, Atmos. Chem. Phys., 14, 3133-3149, 10.5194/acp-14-3133-2014, ~~2014~~2014a.

Xu, J., Zhang, Q., Chen, M., Ge, X., Ren, J., and Qin, D.: Chemical composition, sources, and processes of urban aerosols during summertime in northwest China: insights from high-resolution aerosol mass spectrometry, Atmos. Chem. Phys., 14, 12593-12611, 10.5194/acp-14-12593-2014, 2014b.

Xu, J., Shi, J., Zhang, Q., Ge, X., Canonaco, F., Prévôt, A. S. H., Vonwiller, M., Szidat, S., Ge, J., Ma, J., An, Y., Kang, S., and Qin, D.: Wintertime organic and inorganic aerosols in Lanzhou, China: sources, processes, and comparison with the results during summer, Atmos. Chem. Phys., 16, 14937-14957, 10.5194/acp-16-14937-2016, 2016.

Yanai, M., and Li, C.: Mechanism of heating and the boundary layer over the Tibetan Plateau, Monthly Weather Review, 122, 305-323, 1994.

Yasunari, T. J., Bonasoni, P., Laj, P., Fujita, K., Vuillermoz, E., Marinoni, A., Cristofanelli, P., Duchi, R., Tartari, G., and Lau, K. M.: Estimated impact of black carbon deposition during pre-monsoon season from Nepal Climate Observatory – Pyramid data and snow albedo changes over Himalayan glaciers, Atmos. Chem. Phys., 10, 6603-6615, 10.5194/acp-10-6603-2010, 2010.

Zhang, D., Iwasaka, Y., and Shi, G.: Soot particles and their impacts on the mass cycle in the Tibetan atmosphere, Atmos. Environ., 35, 5883-5894, 10.1016/s1352-2310(01)00391-0, 2001.

Zhang, Q., Jimenez, J. L., Canagaratna, M. R., Ulbrich, I. M., Ng, N. L., Worsnop, D. R., and Sun, Y.: Understanding atmospheric organic aerosols via factor analysis of aerosol mass spectrometry: a review, Anal. Bioanal. Chem., 401, 3045-3067, 10.1007/s00216-011-5355-y, 2011.

Zhang, R., Wang, H., Qian, Y., Rasch, P. J., Easter, R. C., Ma, P. L., Singh, B., Huang, J., and Fu, Q.: Quantifying sources, transport, deposition, and radiative forcing of black carbon over the Himalayas and Tibetan Plateau, Atmos. Chem. Phys., 15, 6205-6223, 10.5194/acp-15-6205-2015, 2015.

Zhang, R., Wang, Y., He, Q., Chen, L., Zhang, Y., Qu, H., Smeltzer, C., Li, J., Alvarado, L. M. A., Vrekoussis, M., Richter, A., Wittrock, F., and Burrows, J. P.: Enhanced trans-Himalaya pollution transport to the Tibetan Plateau by cut-off low systems, Atmos. Chem. Phys., 17, 3083-3095, 10.5194/acp-17-3083-2017, 2017.

Zhao, Z., Cao, J., Shen, Z., Xu, B., Zhu, C., Chen, L. W. A., Su, X., Liu, S., Han, Y., Wang, G., and Ho, K.: Aerosol particles at a high-altitude site on the Southeast Tibetan Plateau, China: Implications for pollution transport from South Asia, J. Geophys. Res.-Atmos., 118, 11360-11375, 10.1002/jgrd.50599, 2013.

Zhou, S., Collier, S., Jaffe, D. A., Briggs, N. L., Hee, J., Sedlacek Iii, A. J., Kleinman, L., Onasch, T. B., and Zhang, Q.: Regional influence of wildfires on aerosol chemistry in the western US and insights into atmospheric aging of biomass burning organic aerosol, Atmos. Chem. Phys., 17, 2477-2493, 10.5194/acp-17-2477-2017, 2017.

774 Table 1. Summary of AMS measurement at mountain sites around the world. The mass

775 concentration was for NR-PM$_1$.

Sites	Instruments	Lat.	Long.	Elev.	Date	Mass Conc.	Reference
Nam Co	HR-AMS	30.77°N	90.9°E	4730	Jun-15	1.84	
Menyuan	ACSM	37.61°N	101.26°E	3925	5 September – 15 October, 2013	10.8	Du et al. (2015)
Montsec	ACSM	42.05°N	0.73°E	1570	14 July 2011 - 23 April 2012	4.9	Rinaldi et al. (2015)
Jungfraujoch	ToF-ACSM	46.55°N	07.98°E	3580	27 July 2012 - 2 October 2013	0.55	Fröhlich et al. (2015)
Mt. Cimone	HR-AMS	44.18°N	10.7°E	2165	June - July 2012	4.5	Rinaldi et al. (2015)
Mt. Whistler	HR-AMS	50.01°N	122.95°E	2182	Apr - May 2006	1.91	Sun et al. (2009)
Puy de Done	cToF-AMS	45.77°N	2.95°E	1465	Sep 2008 - June 2010	2008 Autumn: 7.82 2008 Winter: 5.58 2009 Summer: 27.594	Freney et al. (2011)
Mt. Bachelor	HR-AMS	43.98°S	121.69W	2800	25 July - 25 August, 2013	15.1	Zhou et al. (2017)
Sub-Antarctic Bird Island	HR-AMS	54.00°S	38.00°W	ND	November and December, 2010	0.46	Schmale et al. (2013)

776

777

778
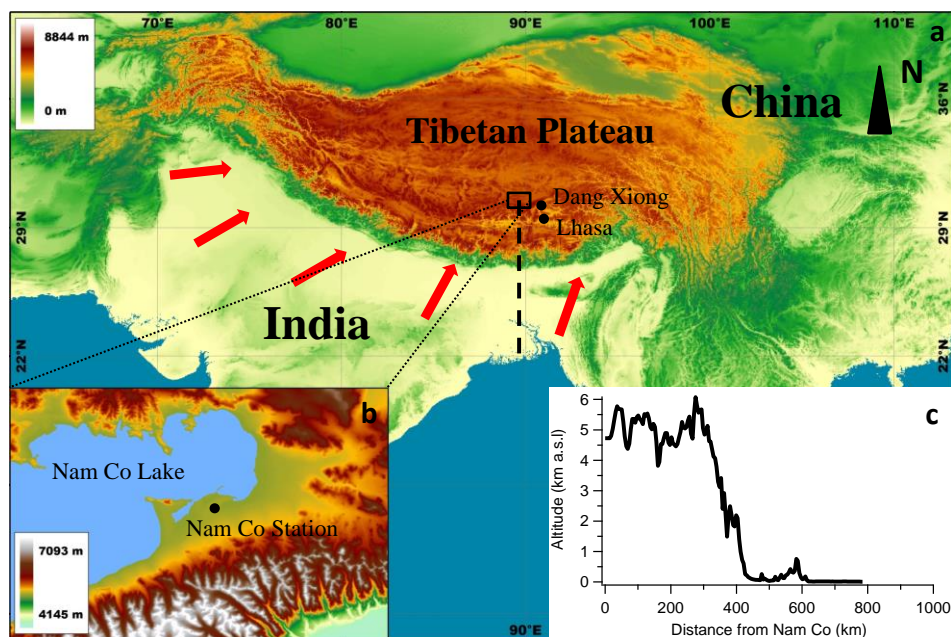
Figure 1. Location map for (a) the Tibetan Plateau and (b) Nam Co Station colored by the
~~elevation.~~altitude. (c) The ~~elevation~~ profile of altitude from costal area to Nam Co Station
(vertical dash line). The red arrow in the map represent the possible wind direction.

782

783

784

785
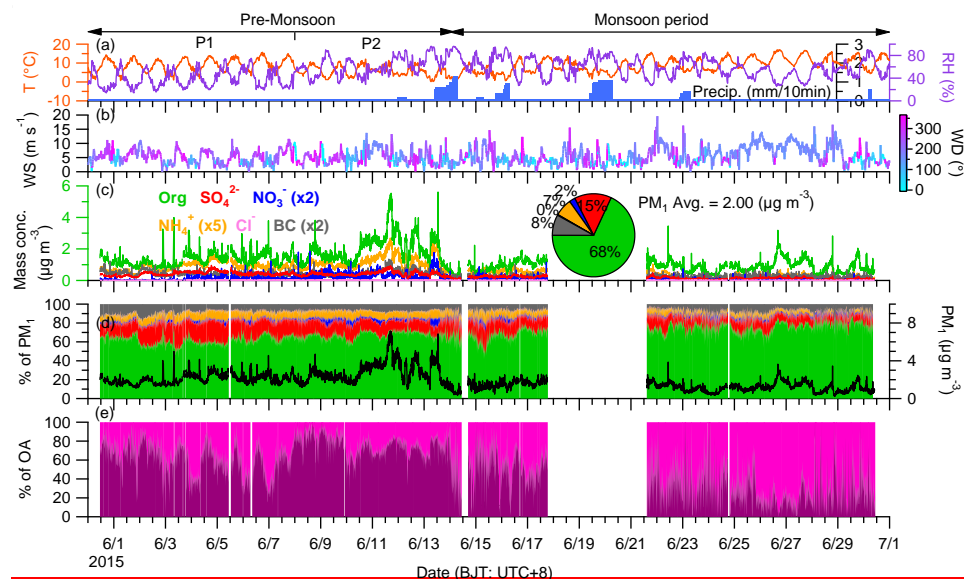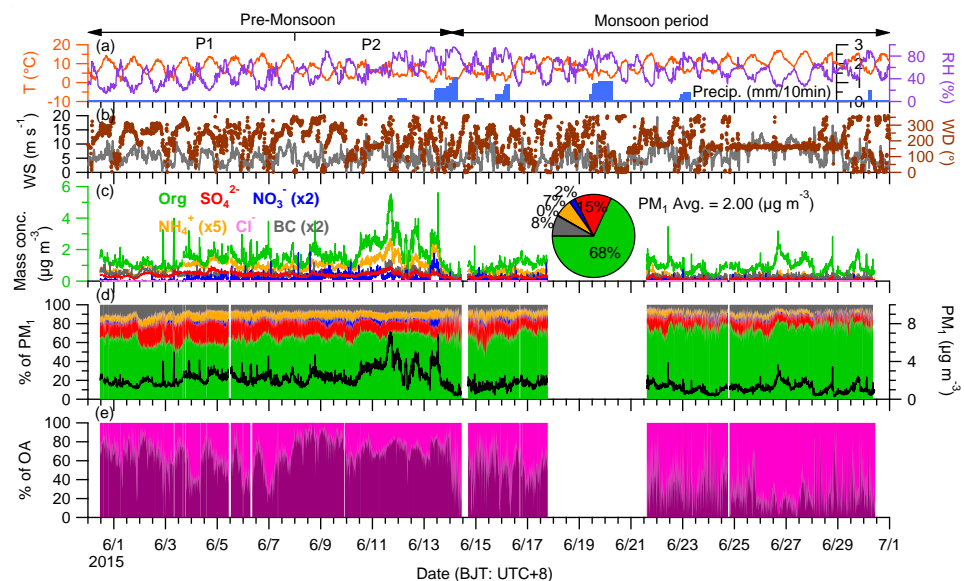
Figure 2. The combo plot of the data of the Nam Co study including (a) the meteorological conditions (T: air temperature; RH: relative humidity; Precip.: precipitation), (b) the variation of WS (wind speed) colored by WD (wind direction), (c) the temporal variation of mass concentration of PM_1 species and the average contribution each species (pie chart), (d) the mass contribution of each PM_1 species and the total mass

790 concentration of PM_1, and (e) the mass contribution of PMF results (section 3.5). Three periods based on

791 the meteorological conditions were marked.

792
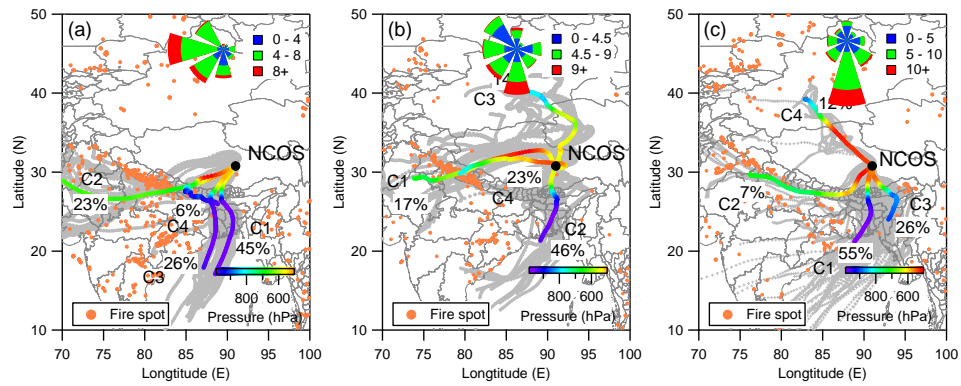
Figure 3. Air mass trajectory statistics for (a) P1, (b) P2, and (c) monsoon period. The classes of trajectories are colored by pressure. Fire spot observed by MODIS and average wind rose plot during each period are also shown.
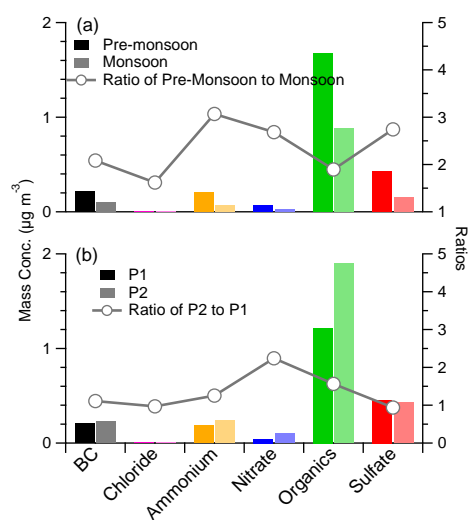
797
798 Figure 4. The comparisons of PM_1 species of the mass concentration (left axis) and the ratio between them
799 (right axis) between (a) pre-monsoon and monsoon and (b) P1 and P2.
800
801

802
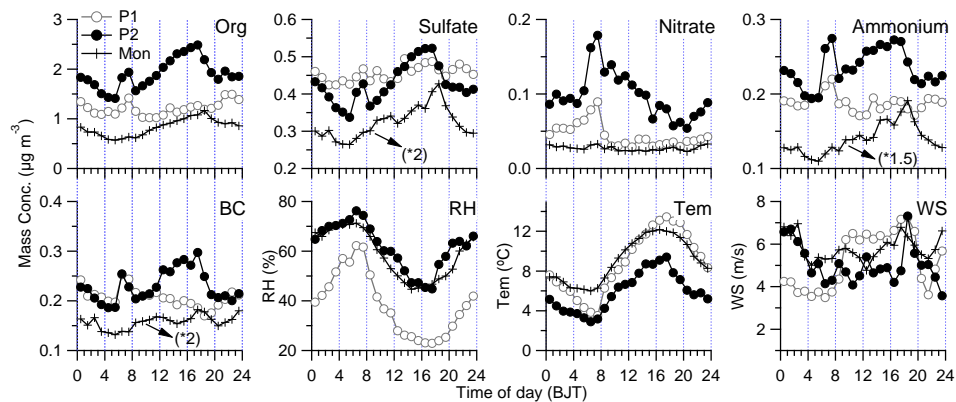
803
804 Figure 5. Diurnal variations of each species and weather conditions (RH: relative humidity; Tem: air
805 temperature; and WS: wind speed) during three periods of the study. Note that the signals of sulfate,
806 ammonium, and BC are increased by a factor for comparison.
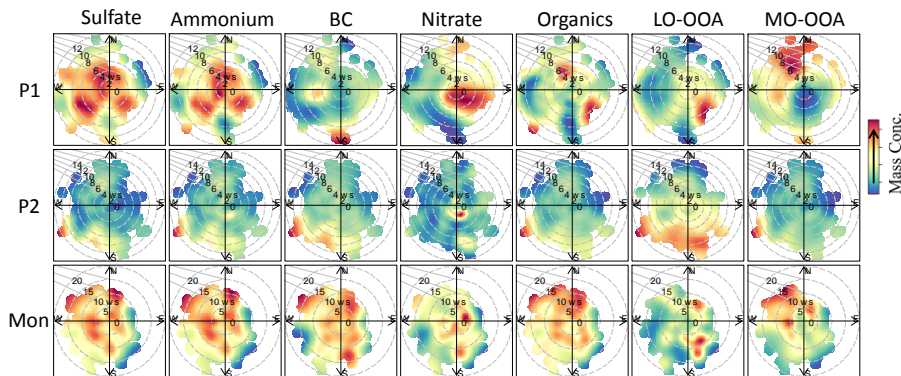
809   Figure 6. Bivariate polar plots that illustrate the variations of the concentrations (colored) of each species as

810   a function of wind speed (m s^{-1}) and wind direction during different periods of the study.

811
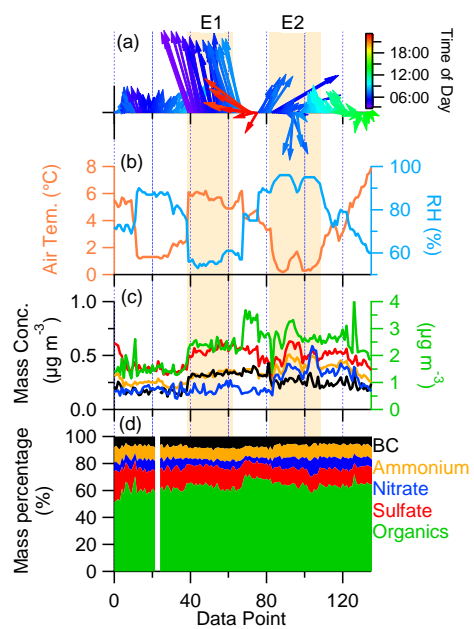
812
813 Figure 7. The high aerosol loading periods based on nitrate (> average + 2σ) accompanying with
814 meteorological data.
815

816

817
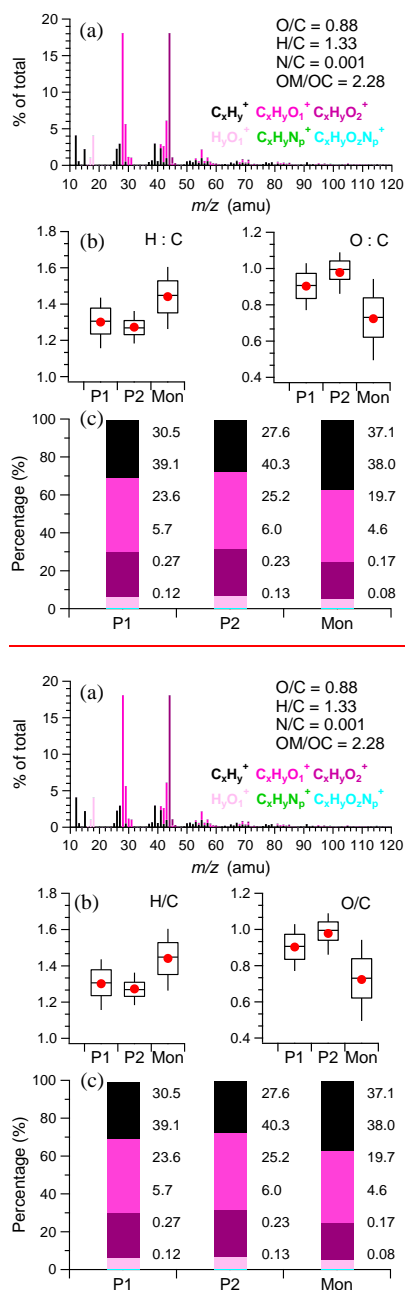
818   Figure 8. (a) The average mass spectrum of organic aerosol, (b) the average ratios of H÷/C and O÷/C

819   during different periods, and (c) the average contribution of six ion categories during different periods.

820

821
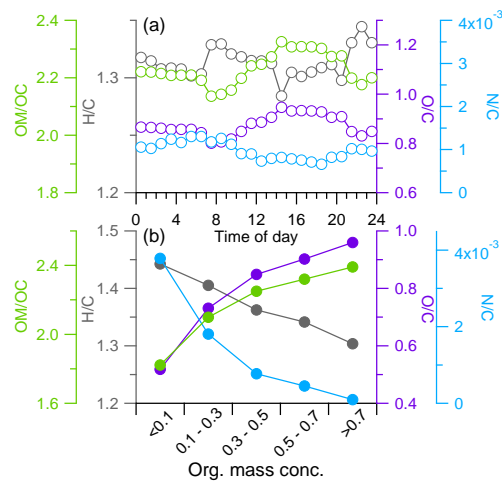
823
824 Figure 9. (a) Diurnal variations of elemental ratios and (b) the variations of elemental ratios as the function
825 of mass concentration of organic aerosol.
826

827
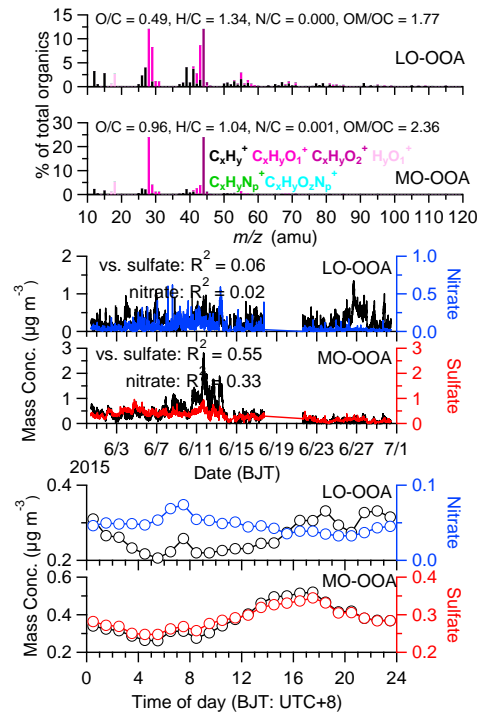
828

829 Figure 10. PMF results of (a) the mass spectra, (b) the temporal variation and (c) diurnal variations of two

830 factors. The temporal and diurnal variations of sulfate and nitrate are also shown for comparisons.

831

832
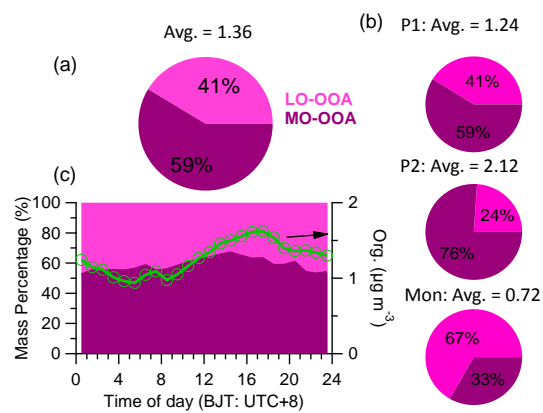
835 Figure 11. (a) The average mass contributions of two factors (a) during the study, (b) during the different

836 periods, and (c) the diurnal mass contribution of two factor (left axis) accompanying with the total organics

837 (right axis).

838

839

840
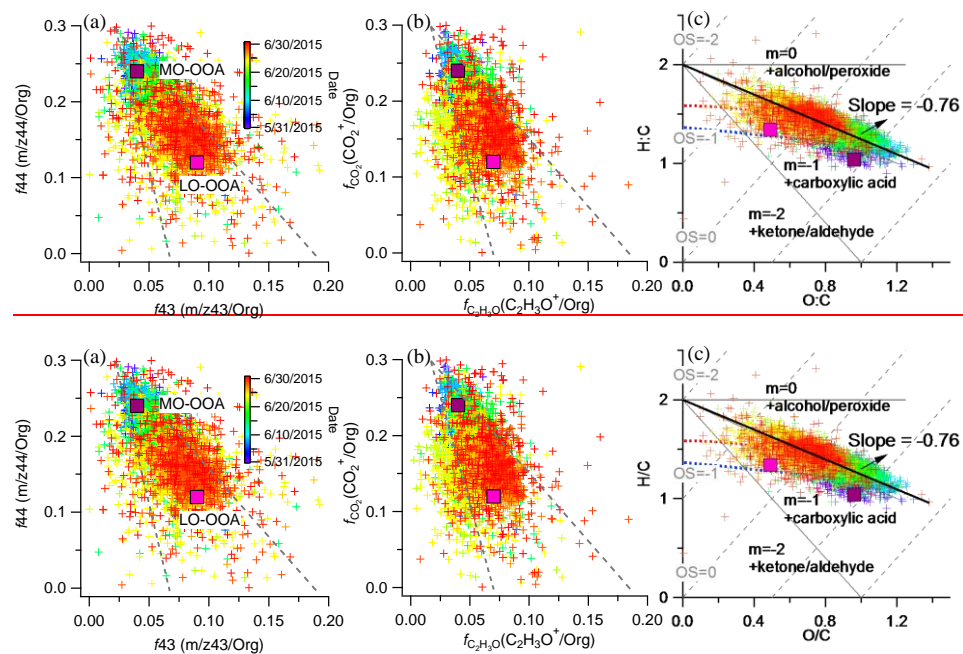
Figure 12. Scatter plots of (a) $f44$ vs. $f43$, (b) fCO_2^+ vs. $fC_2H_3O^+$, and (c) H:/C vs. O:/C for the OA. The corresponding values of the OOAs identified in this study are also shown.

843
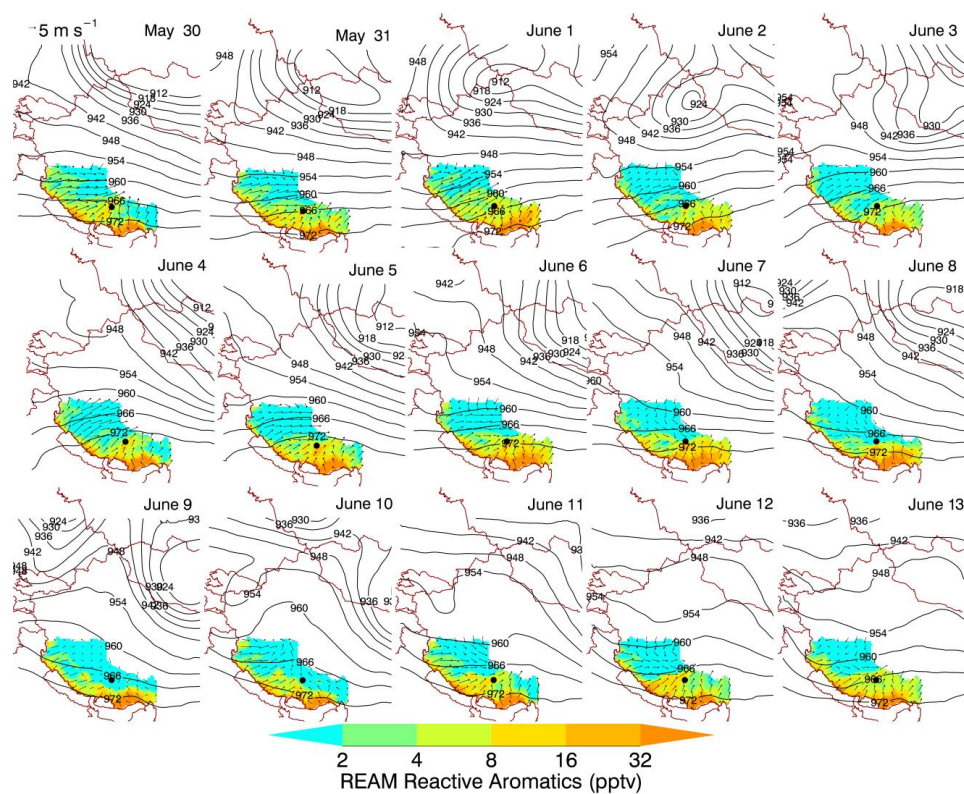
844 Figure 13. Daily distribution of WRF-simulated surface wind and REAM-simulated

845 concentrations of reactive aromatics over the Tibet Plateau during 30 May to 13 June, 2015.

846

Supplementary of:

Chemical characteristics of submicron-particle at the central Tibet Plateau: ~~influence of long-range transport~~insights from aerosol mass spectrometry

Jianzhong Xu[1], Qi Zhang[2], Jinsen Shi[3], Xinlei Ge[4], Conghui Xie[1], Junfeng Wang[4], Shichang Kang[1], Ruxiong Zhang[5], Yuhang Wang[5]

[1]State Key Laboratory of Cryospheric Sciences, Northwest Institute of Eco-Environment and Resources, CAS, Lanzhou 730000, China

[2]Department of Environmental Toxicology, University of California, Davis, CA 95616, USA

[3]Key Laboratory for Semi-Arid Climate Change of the Ministry of Education, College of Atmospheric Sciences, Lanzhou University, Lanzhou 730000, China

[4]Jiangsu Key Laboratory of Atmospheric Environment Monitoring and Pollution Control (AEMPC), School of Environmental Science and Engineering, Nanjing University of Information Science & Technology, Nanjing 210044, China

[5]School of Earth and Atmospheric Sciences, Georgia Institute of Technology, Atlanta, GA, USA

Model description

The 3-D Regional chEmical trAnsport Model (REAM) has a horizontal resolution of 36 km. REAM features 30 vertical layers in the troposphere and 5 vertical layers in the stratosphere, with a model top at 10 hpa. Meteorological fields in REAM are from Weather Research and Forecast model (WRF) assimilations, and are updated every 5 minutes for convective transport related inputs and every 30 minutes for the others. The WRF model is constrained by National Centers for Environmental Prediction Climate Forecast System Reanalysis (NCEP CFSR, Saha et al., 2010) 6-hourly products. The initial and boundary conditions for chemical tracers in REAM are obtained from GEOS-Chem global simulations with a resolution of $2° \times 2.5°$ (Bey et al., 2001). REAM expands GEOS-Chem standard chemical mechanism (v9-02) with aromatic chemistry (Liu et al., 2010, 2012), including benzene and other reactive aromatics as chemical tracers (toluene, ethyl-benzene, and m/p/o-xylene). REAM implements the Intercontinental Chemical Transport Experiment-Phase B (INTEX-B) anthropogenic emissions inventory for South Asia (Zhang et al., 2009; Li et al., 2014) and a mosaic Asian anthropogenic emissions inventory (MIX, Li et al., 2015) for other regions in the model domain. For further model descriptions and evaluations, we refer readers to Zhang et al. (2017).
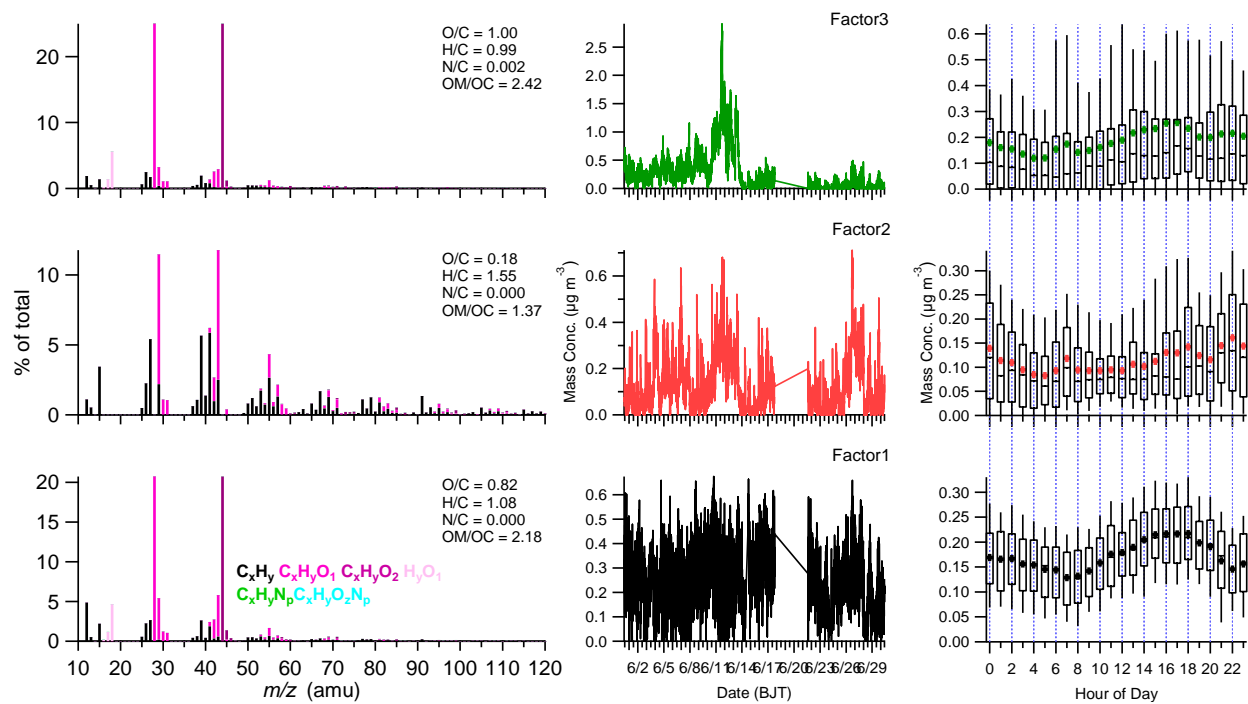
35   Figure S1 Three factor solutions.
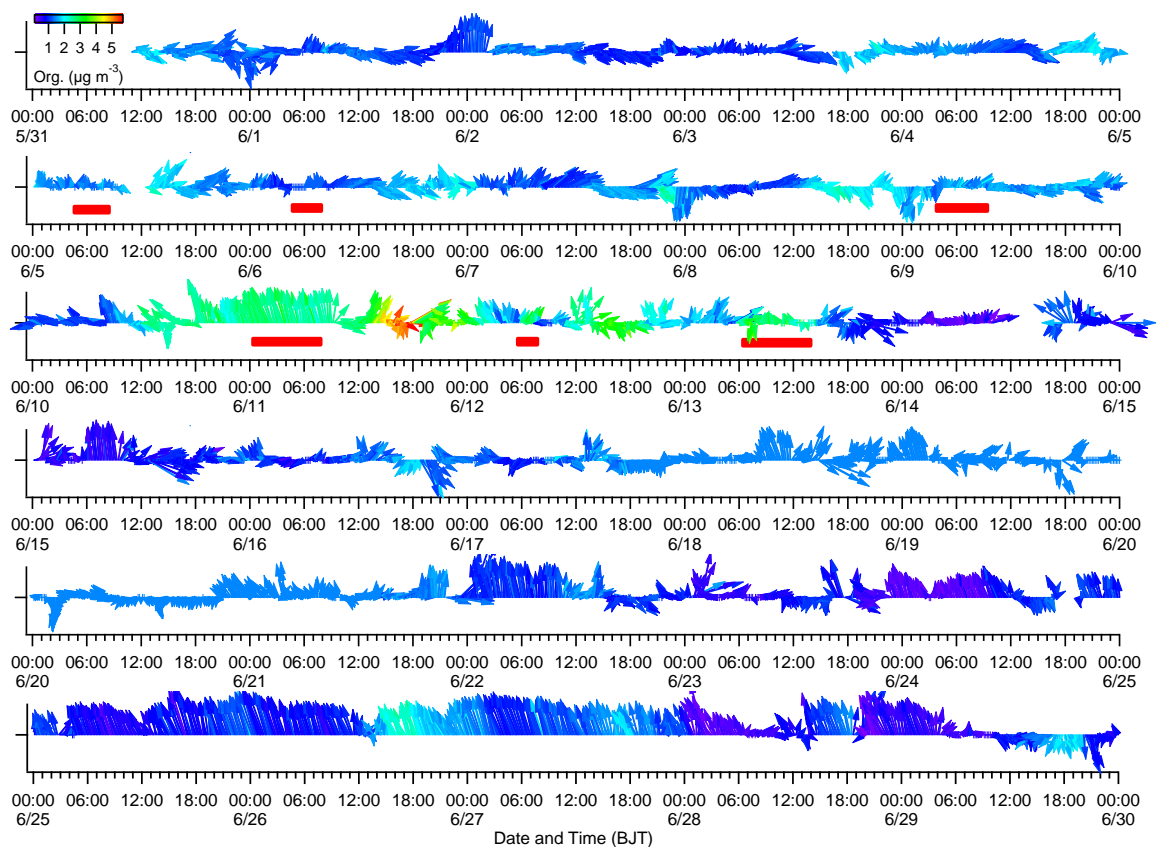
39   Figure S2. The wind dataset during field study. The red marker along the wind represent the high nitrate periods.
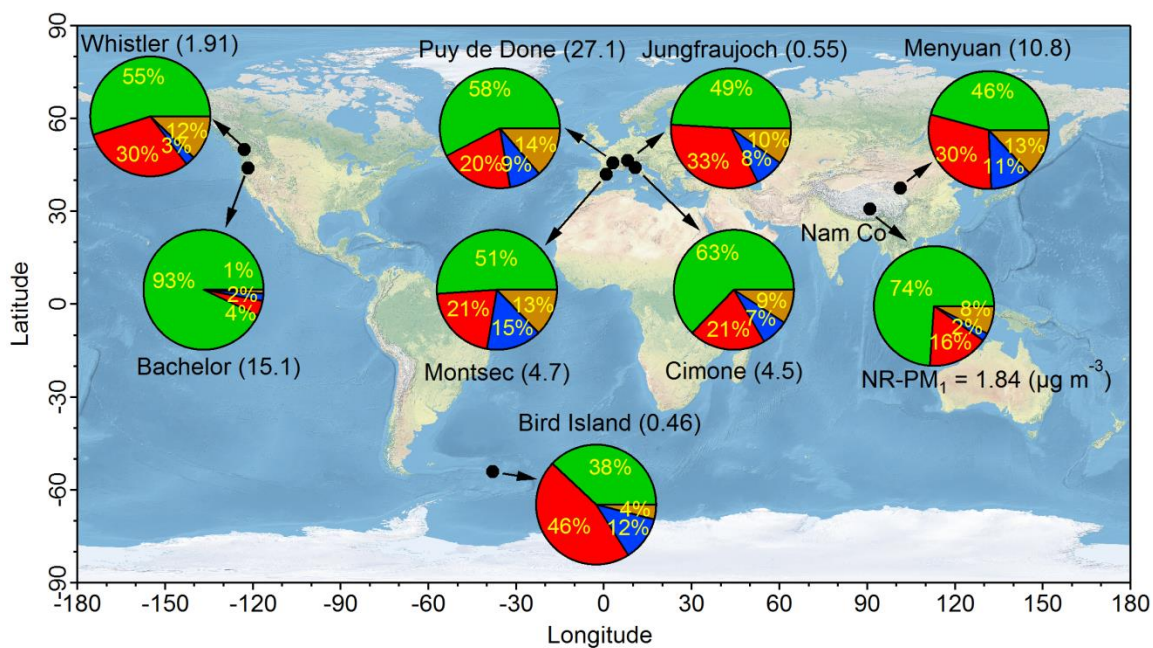
42 Figure S3. The field studies conducted at high elevation sites using AMS. The mass concentration of NR-PM$_1$ and

43 the mass contribution of each species (pie chart) are including in each site.
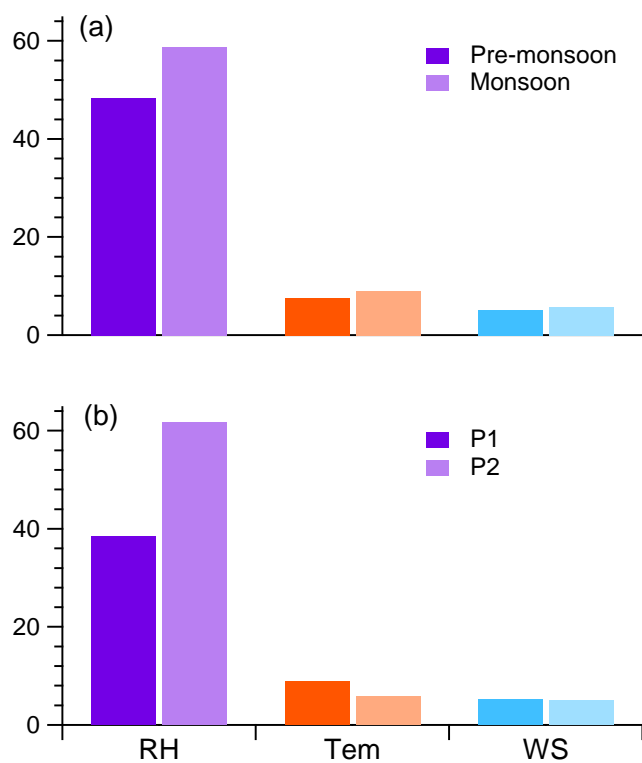
46   Figure S4. The comparisons of meteorological conditions between (a) pre-monsoon and monsoon and (b) P1 and P2.

50
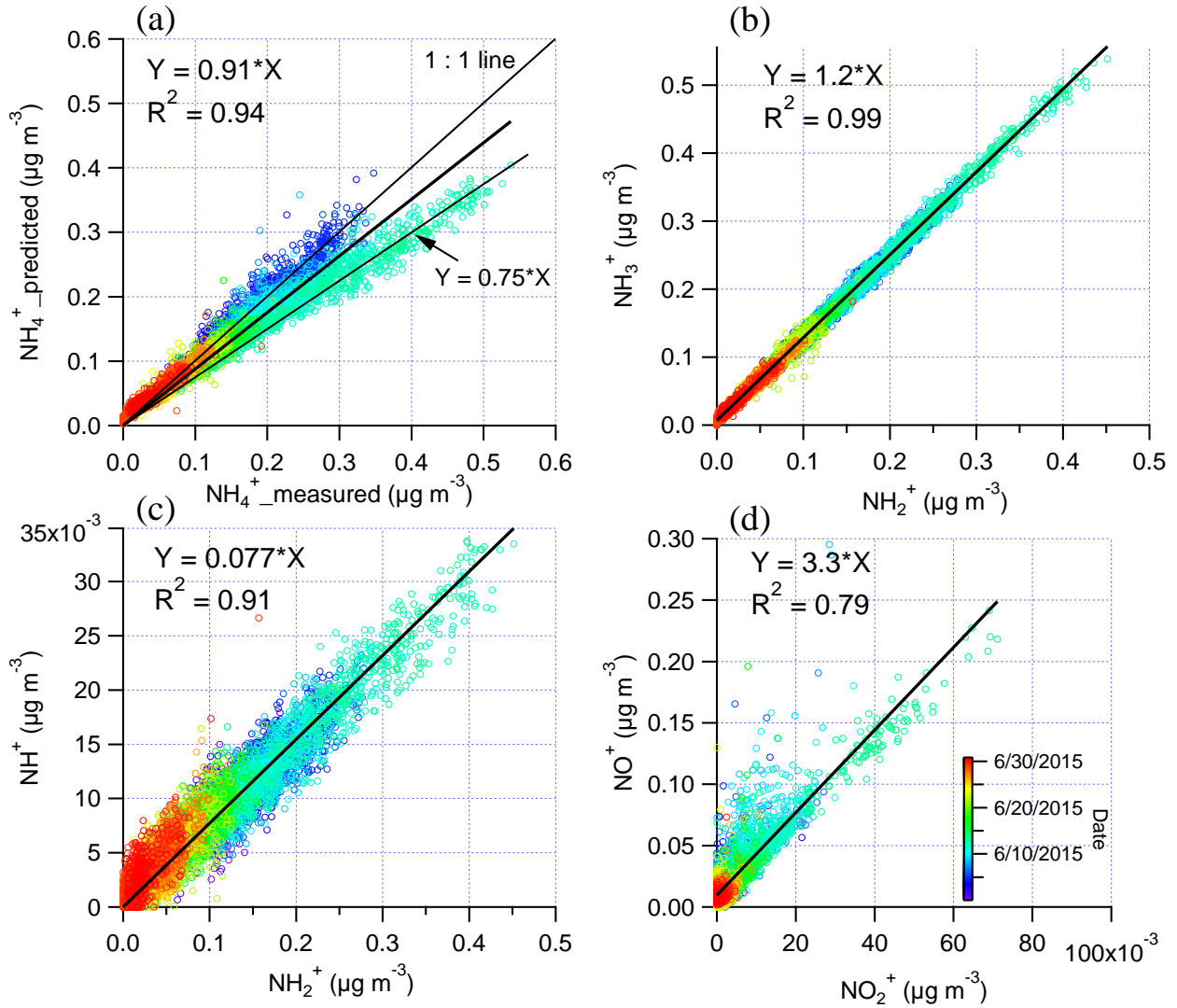
51 Figure S5. Scatter plots of (a) predicted ammonium (NH$_4^+$_predicted) calculated from the stoichiometry of sulfate,

52 nitrate, and chloride vs. measured ammonium (NH$_4^+$_measured), (b) NH$_3^+$ vs. NH$_2^+$, (c) NH$^+$ vs. NH$_2^+$, and (d) NO$^+$

53 vs. NO$_2^+$.

54

55

56
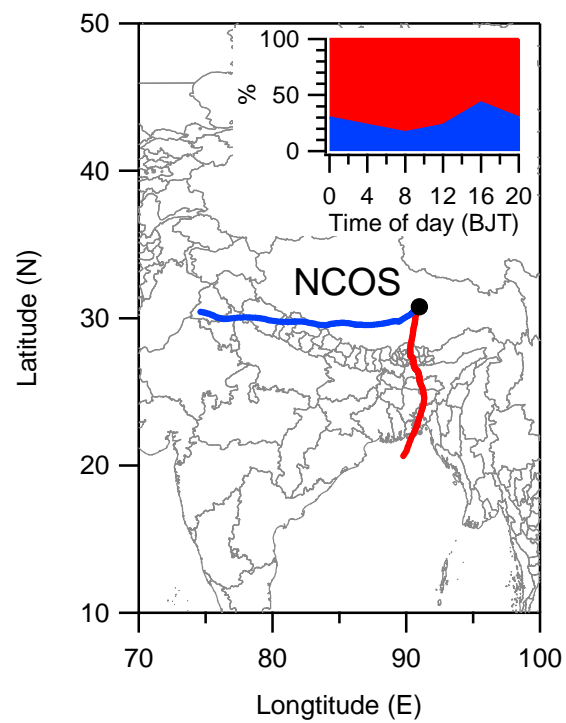
57   Figure S6. The diurnal contribution of two class air trojectories arrived at Nam Co during sampling period.

58

59
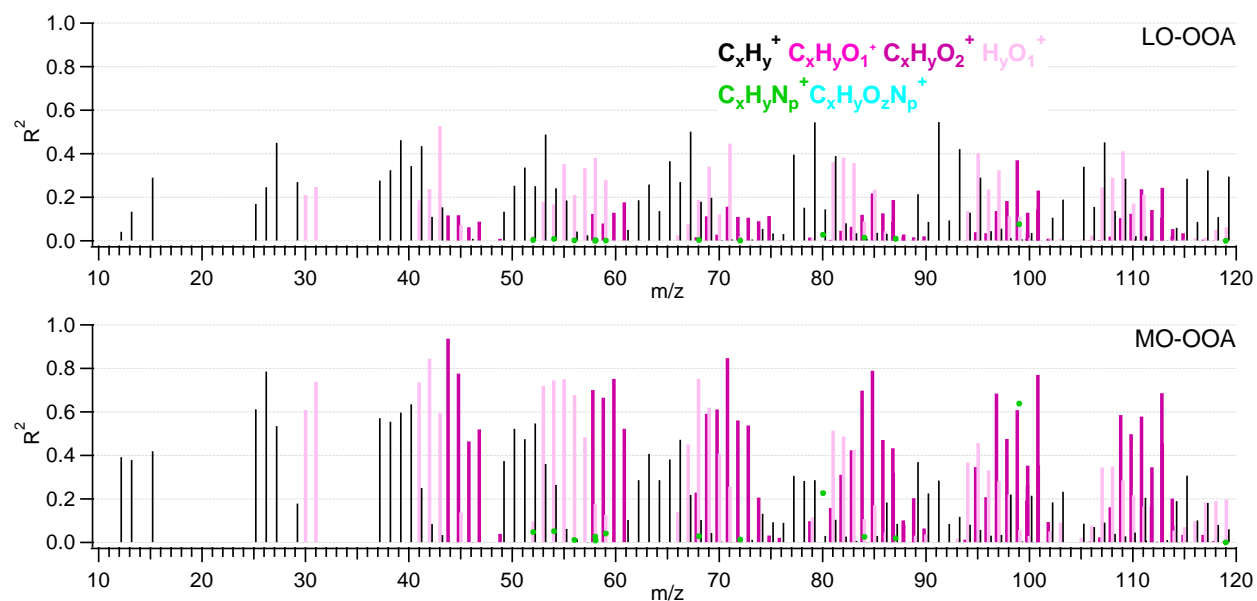
60   Figure S7. The correlation coefficent of time series between OOA factor and ions.

61

62
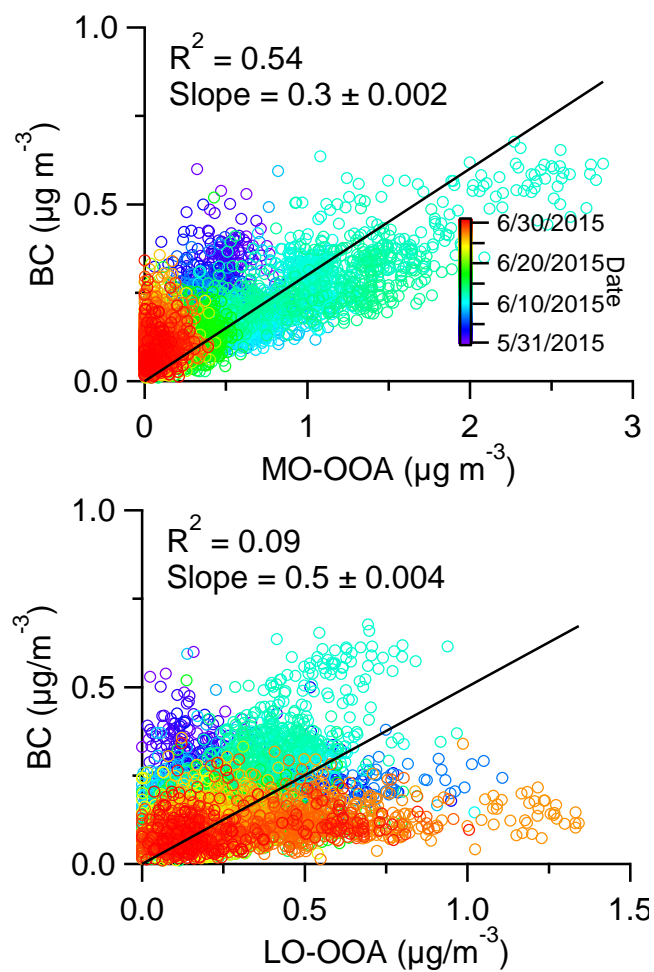
63   Figure S8. Scatter plots between BC and OOA factors.

64

65

66
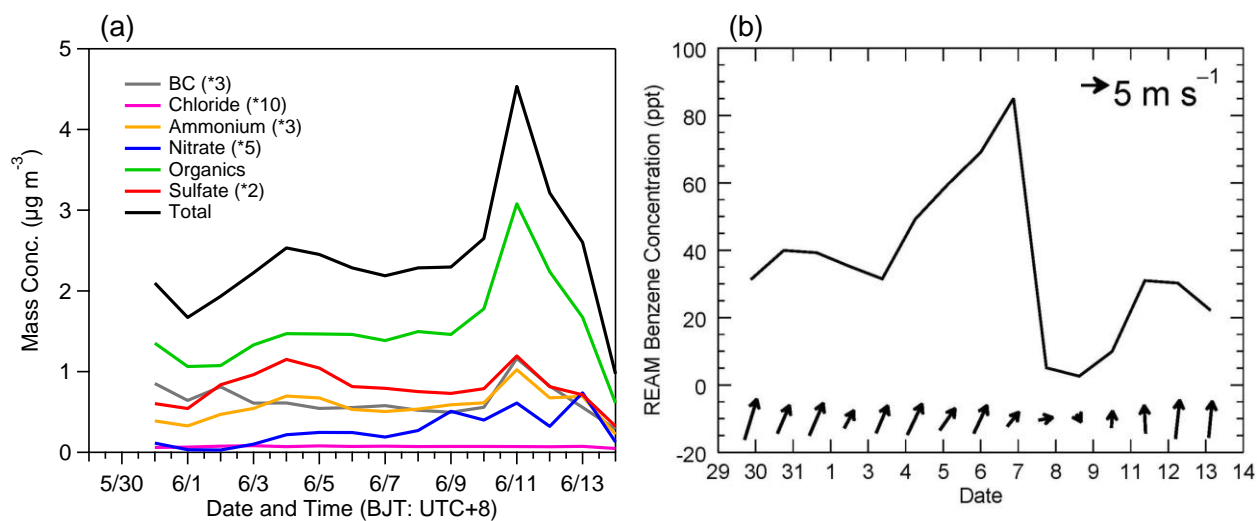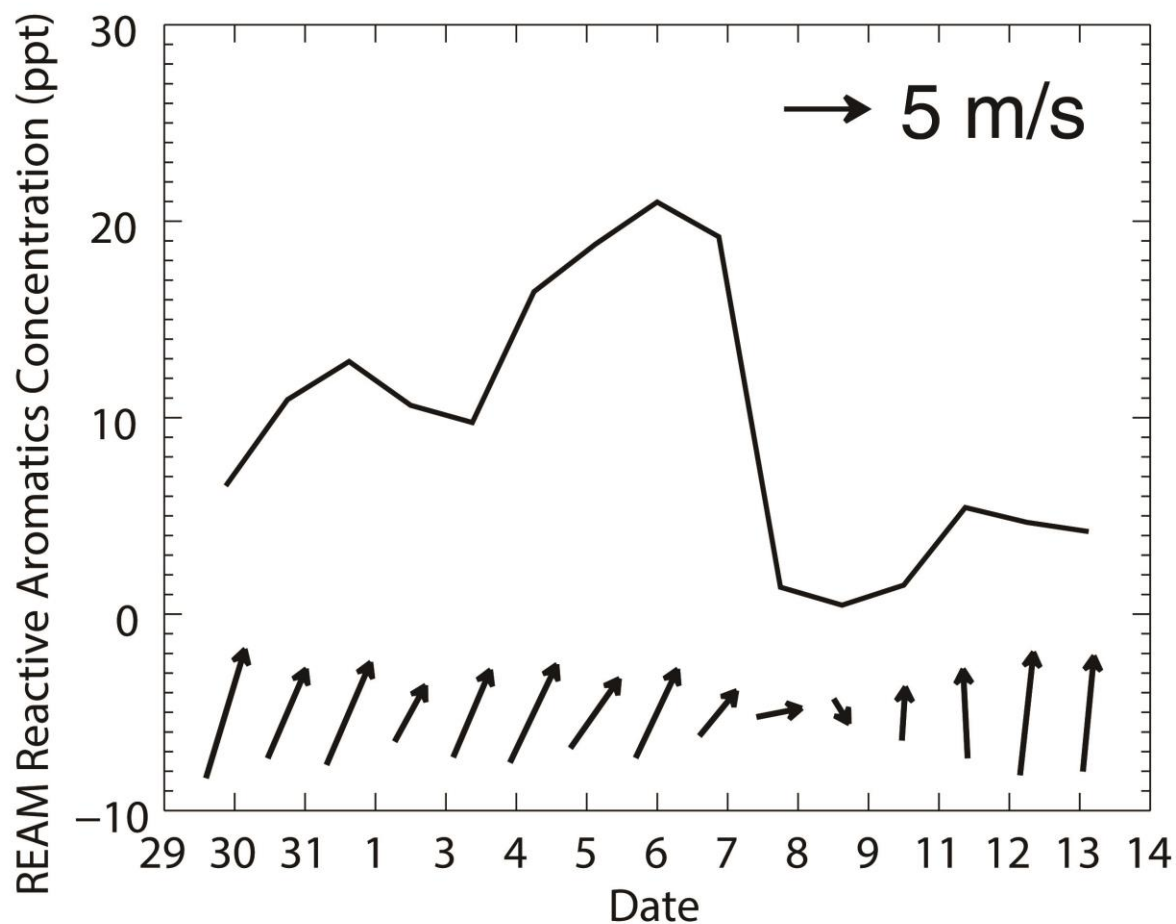
Figure S9. The mass concentration of (a) AMS results and (b) REAM-simulated reactive aromatics and the averaged

wind data.

69

71   **References**

72   Bey, I., Jacob, D. J., Yantosca, R. M., Logan, J. A., Field, B. D., Fiore, A. M., Li, Q. B., Liu, H. G. Y.,
73   Mickley, L. J., and Schultz, M. G.: Global modeling of tropospheric chemistry with assimilated
74   meteorology: Model description and evaluation, J. Geophys. Res.-Atmos., 106, 23073-23095, doi:
75   10.1029/2001jd000807, 2001.

76   Li, M., Zhang, Q., Streets, D. G., He, K. B., Cheng, Y. F., Emmons, L. K., Huo, H., Kang, S. C., Lu, Z.,
77   Shao, M., Su, H., Yu, X., and Zhang, Y.: Mapping Asian anthropogenic emissions of non-
78   methane volatile organic compounds to multiple chemical mechanisms, Atmos. Chem. Phys., 14,
79   5617-5638, doi: 10.5194/acp-14-5617-2014, 2014.

80   Li, M., Zhang, Q., Kurokawa, J., Woo, J. H., He, K. B., Lu, Z., Ohara, T., Song, Y., Streets, D. G.,
81   Carmichael, G. R., Cheng, Y. F., Hong, C. P., Huo, H., Jiang, X. J., Kang, S. C., Liu, F., Su, H.,
82   and Zheng, B.: MIX: a mosaic Asian anthropogenic emission inventory for the MICS-Asia and
83   the HTAP projects, Atmos. Chem. Phys. Discuss., 2015, 34813-34869, doi: 10.5194/acpd-15-
84   34813-2015, 2015.

85   Liu, Z., Wang, Y., Gu, D., Zhao, C., Huey, L. G., Stickel, R., Liao, J., Shao, M., Zhu, T., Zeng, L., Liu,
86   S.-C., Chang, C.-C., Amoroso, A., and Costabile, F.: Evidence of Reactive Aromatics As a Major
87   Source of Peroxy Acetyl Nitrate over China, Environ. Sci. Technol., 44, 7017-7022, doi:
88   10.1021/es1007966, 2010.

89   Liu, Z., Wang, Y., Vrekoussis, M., Richter, A., Wittrock, F., Burrows, J. P., Shao, M., Chang, C.-C., Liu,
90   S.-C., Wang, H., and Chen, C.: Exploring the missing source of glyoxal (CHOCHO) over China,
91   Geophys. Res. Lett., 39, L10812, doi: 10.1029/2012GL051645, 2012.

92   Saha, S., Moorthi, S., Pan, H.-L., Wu, X., Wang, J., Nadiga, S., Tripp, P., Kistler, R., Woollen, J.,
93   Behringer, D., Liu, H., Stokes, D., Grumbine, R., Gayno, G., Wang, J., Hou, Y.-T., Chuang, H.-
94   Y., Juang, H.-M. H., Sela, J., Iredell, M., Treadon, R., Kleist, D., Van Delst, P., Keyser, D.,
95   Derber, J., Ek, M., Meng, J., Wei, H., Yang, R., Lord, S., Van Den Dool, H., Kumar, A., Wang,
96   W., Long, C., Chelliah, M., Xue, Y., Huang, B., Schemm, J.-K., Ebisuzaki, W., Lin, R., Xie, P.,
97   Chen, M., Zhou, S., Higgins, W., Zou, C.-Z., Liu, Q., Chen, Y., Han, Y., Cucurull, L., Reynolds,
98   R. W., Rutledge, G., and Goldberg, M.: The NCEP Climate Forecast System Reanalysis, Bull.
99   Am. Meteorol. Soc., 91, 1015-1057, doi: 10.1175/2010BAMS3001.1, 2010.

100   Zhang, Q., Streets, D. G., Carmichael, G. R., He, K. B., Huo, H., Kannari, A., Klimont, Z., Park, I. S.,
101   Reddy, S., Fu, J. S., Chen, D., Duan, L., Lei, Y., Wang, L. T., and Yao, Z. L.: Asian emissions in
102   2006 for the NASA INTEX-B mission, Atmos. Chem. Phys., 9, 5131-5153, doi: 10.5194/acp-9-
103   5131-2009, 2009.

104   Zhang, R., Wang, Y., He, Q., Chen, L., Zhang, Y., Qu, H., Smeltzer, C., Li, J., Alvarado, L. M. A.,
105   Vrekoussis, M., Richter, A., Wittrock, F., and Burrows, J. P.: Enhanced trans-Himalaya pollution
106   transport to the Tibetan Plateau by cut-off low systems, Atmos. Chem. Phys., 17, 3083-3095,
107   10.5194/acp-17-3083-2017, 2017.

108